Integrating single-cell RNA-seq to identify fibroblast-based molecular subtypes for predicting prognosis and therapeutic response in bladder cancer

Jia Wang[1,2], Zhiyong Tan[3], Yinglong Huang[3], Charles Li[4,5,6], Peiqin Zhan[1,3], Haifeng Wang[1,3], Haihao Li[1,3]

[1]The Second Clinical Medical College, Kunming Medical University, Kunming, China
[2]Department of Endocrinology, The Second Affiliated Hospital of Kunming Medical University, Kunming, China
[3]Department of Urology, The Second Affiliated Hospital of Kunming Medical University, Kunming, China
[4]Core Facility for Protein Research, Chinese Academy of Sciences, Beijing, China
[5]Zhongke Jianlan Medical Research Institute, Beijing, China
[6]Zhejiang Institute of Integrated Traditional and Western Medicine, Hangzhou, China

Correspondence to: Haifeng Wang, Haihao Li; **email:** wanghaifeng@kmmu.edu.cn, lihaihao@kmmu.edu.cn
Keywords: scRNA-seq, bladder cancer, prognostic signature, fibroblast cell, immunotherapy response
Received: January 9, 2024 **Accepted:** July 5, 2024 **Published:** July 18, 2024

ABSTRACT

Background: Bladder cancer (BLCA) is a highly aggressive and heterogeneous disease, posing challenges for diagnosis and treatment. Cancer immunotherapy has recently emerged as a promising option for patients with advanced and drug-resistant cancers. Fibroblasts, a significant component of the tumor microenvironment, play a crucial role in tumor progression, but their precise function in BLCA remains uncertain.

Methods: Single-cell RNA sequencing (scRNA-seq) data for BLCA were obtained from the Gene Expression Omnibus database. The R package "Seurat" was used for processing scRNA-seq data, with uniform manifold approximation and projection (UMAP) for downscaling and cluster identification. The FindAllMarkers function identified marker genes for each cluster. Differentially expressed genes influencing overall survival (OS) of BLCA patients were identified using the limma package. Differences in clinicopathological characteristics, immune microenvironment, immune checkpoints, and chemotherapeutic drug sensitivity between high- and low-risk groups were investigated. RT-qPCR and immunohistochemistry validated the expression of prognostic genes.

Results: Fibroblast marker genes identified three molecular subtypes in the testing set. A prognostic signature comprising ten genes stratified BLCA patients into high- and low-score groups. This signature was validated in one internal and two external validation sets. High-score patients exhibited increased immune cell infiltration, elevated chemokine expression, and enhanced immune checkpoint expression but had poorer OS and a reduced response to immunotherapy. Six sensitive anti-tumor drugs were identified for the high-score group. RT-qPCR and immunohistochemistry showed that CERCAM, TM4SF1, FN1, ANXA1, and LOX were highly expressed, while EMP1, HEYL, FBN1, and SLC2A3 were downregulated in BLCA.

Conclusion: A novel fibroblast marker gene-based signature was established, providing robust predictions of survival and immunotherapeutic response in BLCA patients.

INTRODUCTION

Bladder cancer (BLCA) is the 10th most common cancer worldwide, with uroepithelial carcinoma accounting for about 90% of cases. In 2020, there were approximately 573,000 new cases and 213,000 deaths globally [1, 2]. Despite various treatments, the prognosis for BLCA patients remains poor, with a median overall survival (OS) of just 14 months [3]. Chemotherapy is a key first-line treatment, but many patients eventually develop chemoresistance and experience tumor recurrence. Potential mechanisms behind this include enhanced chemoresistance in bladder cancer stem cells (CSCs) and the regulatory inactivation of oncogenes and tumor suppressor genes [4, 5].

Immune checkpoint inhibitors (ICIs) have become important for treating advanced and cisplatin-resistant BLCA, with PD-1/PD-L1 inhibitors approved for first- and second-line therapy. However, only a minority of patients benefit from these treatments [6, 7]. Biomarkers like tumor mutation burden (TMB) and immune checkpoint expression are used to predict immunotherapy response [8, 9], but do not fully capture the tumor microenvironment (TME) heterogeneity. Therefore, a tool to accurately predict BLCA prognosis and immunotherapy response is desperately needed.

The TME includes various immune cells, stromal cells, extracellular matrix (ECM) molecules, and cytokines [10]. Changes in the TME composition can significantly affect tumor progression, invasion, and immunotherapy response [11, 12]. Fibroblasts, the main stromal cells in the TME, are transformed into cancer-associated fibroblasts (CAFs) by tumor cell-generated paracrine growth factors [13]. CAFs play roles in tumor cell proliferation, angiogenesis, ECM remodeling, and anti-tumor immunity [14]. They can secrete immunosuppressive cytokines like IL-6, CXCL1, and CXCL12, promoting immune escape or forming physical barriers to immune cell entry through ECM remodeling [15, 16]. BLCA patients with an immune-excluded phenotype due to CAFs and ECM show decreased responses to nivolumab, while muscle-invasive BLCA patients with low CAF levels are more likely to achieve complete pathological remission with neoadjuvant chemotherapy [17].

Given the critical role of fibroblasts in anti-tumor immunity, further research on fibroblasts is essential for new BLCA treatments. Single-cell RNA sequencing (scRNA-seq) allows for the identification of individual immune cell subpopulations in the TME, providing insights into immune cell heterogeneity and molecular characteristics [18]. This study aims to identify fibroblast marker genes and molecular subtypes and establish a prognostic signature by integrating scRNA-seq and bulk RNA-seq data. We evaluated the correlation between the signature and prognosis, clinicopathological features, and immunotherapy response in BLCA patients. Our results offer promising biomarkers and potential therapeutic targets for BLCA patients.

MATERIALS AND METHODS

Data source and processing

A total of 957 BLCA samples were included in this study. The scRNA-seq dataset GSE135337 containing seven primary tumor samples was obtained from the Gene Expression Omnibus (GEO) database (http://www.ncbi.nlm.nih.gov/geo/), and it was utilized to identify marker genes of fibroblasts. The TCGA-BLCA dataset (411 samples) was merged with the GSE13507 dataset (165 samples), which were down-loaded from UCSC Xena (https://xenabrowser.net/) and the GEO database, respectively. Batch effects were corrected with the "limma" and "sva" packages [19], which were used to construct the prognostic signature. To evaluate the predictive value of the prognostic signature for the effectiveness of immunotherapy in patients, the transcriptomic and matched clinical data of patients who underwent anti-PD1 and anti-PD-L1 treatment from the GSE78220 dataset (n=26) and IMvigor210 cohort (n=348) were collected from GEO database and "IMvigor210CoreBiologies" package (http://researchpub.gene.com/IMvigor210CoreBiologies) [20]. This study was approved by the Ethics Committee of the Second Affiliated Hospital of Kunming Medical University (KYD213238).

scRNA-seq analysis

The scRNA-seq data were screened and analyzed using the R package "Seurat" [21]. Firstly, we performed quality control of the scRNA-seq data with the following criteria: 1) exclusion of genes that appeared in fewer than five cells; 2) removal of cells that expressed fewer than 300 genes; 3) elimination of cells with mitochondrial gene expression above 10%; 4) retention of cells with ribosomal genes > 3% and 5) inclusion of cells with hemoglobin genes < 0.1%. We then used the R package "harmony" to reduce batch effects between samples. Subsequently, we normalized the scRNA-seq data using the "ScaleData" and performed principal component analysis (PCA), and the uniform manifold approximation and projection (UMAP) [22] function to reduce the dimensionality. We employed the "FindAllMarkers" function to identify differentially expressed genes in various clusters. Finally, cells were clustered by a resolution of 0.8 and cell annotation was performed by the R package "singleR" [23] combined with manual adjustment.

Consensus clustering analysis

Based on ten fibroblast marker genes, consensus clustering analysis was performed on the samples of the testing set with the R package "ConsensusClusterPlus" [24] to identify fibroblast subtypes. To ensure the stability of the clustering process, we employed a resampling rate of 80% and 1000 repeats. Subsequently, we selected cluster-effective results as the subtypes of BLCA patients based on survival analysis and differential expression of marker genes.

Gene sets variation analysis (GSVA) and immune cell infiltration analysis

For evaluation of differences in pathways between the three subtypes, we downloaded the HALLMARK, Kyoto Encyclopedia of Genes and Genomes (KEGG), and Reactome pathways from the MSigDB database (http://www.gsea-msigdb.org/gsea/index.jsp) and scored them utilizing the R package "GSVA" [25]. Heatmap plots were generated via the "pheatmap" package. To compare the immune cell infiltration between fibroblast subtypes, the immune score, stromal score, and ESTIMATE score of BLCA patients were measured using the R package "ESTIMATE" [26], and the fraction of immune cell infiltration was calculated by "ssGSEA" function of the R package "GSVA".

Construction of prognostic signature based on fibroblast cell marker genes

Firstly, difference analysis was performed for each of the three subtypes, and genes that exhibited a |log2 (fold change)|>1 and p-value<0.05 were considered as differentially expressed genes (DEGs). These DEGs were pooled to create a gene set, which we then subjected to the Gene Ontology (GO)/KEGG analysis using the R package "clusterprofiler" [27]. Next, we conducted univariate Cox regression analysis on all DEGs to identify the ten signature genes with the smallest p-value associated with prognosis. Subsequently, we performed Consensus clustering analysis on the signature genes to obtain two molecular subtypes. Finally, the final signature scores were calculated by the GSVA method based on ten signature genes, and prognostic signatures were established. In addition, the Kaplan-Meier survival curve was generated using the R package "survminer" (https://CRAN.R-project.org/package=survminer) to compare the differences in OS between high- and low-score groups.

Relationship between prognostic signature and immunotherapy

To elucidate the relationship between risk score and tumor immune microenvironment, correlation analysis

was used to assess the relationship between risk score and immune cell infiltration, as well as 50 hallmark pathways. A significant correlation was defined as p<0.05. Moreover, the expression of multiple chemokines and immune checkpoints was compared between high- and low-score groups to reveal the relationship between risk score and immunotherapy. As TMB is closely related to immunotherapy efficacy, we analyzed the TMB levels between the two groups by the R package "maftools" [28]. In addition, the predictive ability of risk scores for immunotherapy was verified in the internal validation set GSE13507 and the external validation set GSE78220 and IMvigor210, respectively.

Drug sensitivity analysis

To investigate potential treatment options for immunotherapy-insensitive patients, we directed our attention toward targeted therapies. We estimated the 50% maximum inhibitory concentration (IC_{50}) of each sample to multiple anti-cancer drugs using the R package "pRRophetic" [29]. We then compared the differences in IC_{50} values between the high- and low-score groups, where a higher IC_{50} value implies lower sensitivity to treatment.

Quantitative real-time PCR (RT-qPCR) assays

To validate mRNA levels, we performed RT-qPCR according to the manufacturer's instructions. We purchased a normal bladder uroepithelial cell line (SV-HUC-1) and BLCA cell lines (UM-UC-3, RT4, T24, 5627, SW780, and J82) were purchased from the Shanghai Cell Bank of the Chinese Academy of Sciences and cultured them in Roswell Park Memorial Institute (RPMI) 1640 medium supplemented with 10% fetal bovine serum. We extracted total RNA from BLCA and normal bladder uroepithelial cells using TRIzol reagent (Life Technology, CA, USA) and reverse transcribed it into cDNA using PrimeScript RT Master Mix (Takara, Tokyo, Japan), following the manufacturer's instructions. Glyceraldehyde 3-phosphate dehydrogenase (GAPDH) was used as an internal control. The $2^{-\Delta\Delta Ct}$ method was used to determine relative gene expression levels. Supplementary Table 1 lists all mRNA primers used.

Immunohistochemistry (IHC) staining

A total of 24 pairs of paraffin-embedded BLCA and adjacent samples were obtained from the Second Affiliated Hospital of Kunming Medical University, with approval from the ethics committee and written informed consent from each patient for the use of their materials. The tissue slices were baked at 65° C for 2 hours, followed by dewaxing and antigen retrieval.

Endogenous enzymes were blocked using a 3% hydrogen peroxide solution for 10 minutes at room temperature. The slices were rinsed three times with phosphate buffer solution (PBS) for 3 minutes each time and then blocked with bovine serum albumin. The primary antibody was applied and incubated overnight at 4° C. After washing the slices three times with PBS for 5 minutes each time, the secondary antibody was applied and incubated at 37° C for 30 minutes. Diaminobenzidine was used for color rendering for 5-10 minutes, followed by hematoxylin redyes for 3 minutes. The slices were observed under a microscope, and the integrated optical density (IOD) was measured using Image Pro Plus 6.0 image software. The relative expressions were presented as the average optical density (IOD/positive staining area).

Statistical analysis

All statistical analyses and data visualization were performed using the R software (Version 4.1.1) and GraphPad Prism (Version 9.0). We used Pearson correlation analysis to assess correlations between two continuous variables. The Wilcoxon test was employed to compare differences between two variables, and the Kruskal-Wallis test was used to compare multiple variables. Statistical significance was set at a two-sided p-value < 0.05.

Availability of data and materials

The analyzed datasets generated during the study are available from the corresponding author upon reasonable request.

RESULTS

Identification of fibroblast marker gene expression profiles

After filtering the scRNA-seq data, we obtained information on the range of detected gene numbers, the number of transcripts sequenced, the percentage of mitochondrial/ribosomal/hemoglobin content in each sample, and the top 25 genes with the highest rate (Supplementary Figure 1). After reducing the dimensions, we identified 18 clusters and annotated them into five core cell types: T cells, malignant cells, monocytes, macrophages, fibroblasts, and endothelial cells. 21160 genes and 36532 cells were used for further analysis (Figure 1A). Notably, cluster 13 was defined as a fibroblast subpopulation. Figure 1B depicts the number of cells in each cell type, where the fibroblast subpopulation consists of 249 cells. Differential gene expression analysis was conducted for each cell type, and Figure 1C illustrates the top 5 up and down-regulated genes in each cell type. A detailed list of
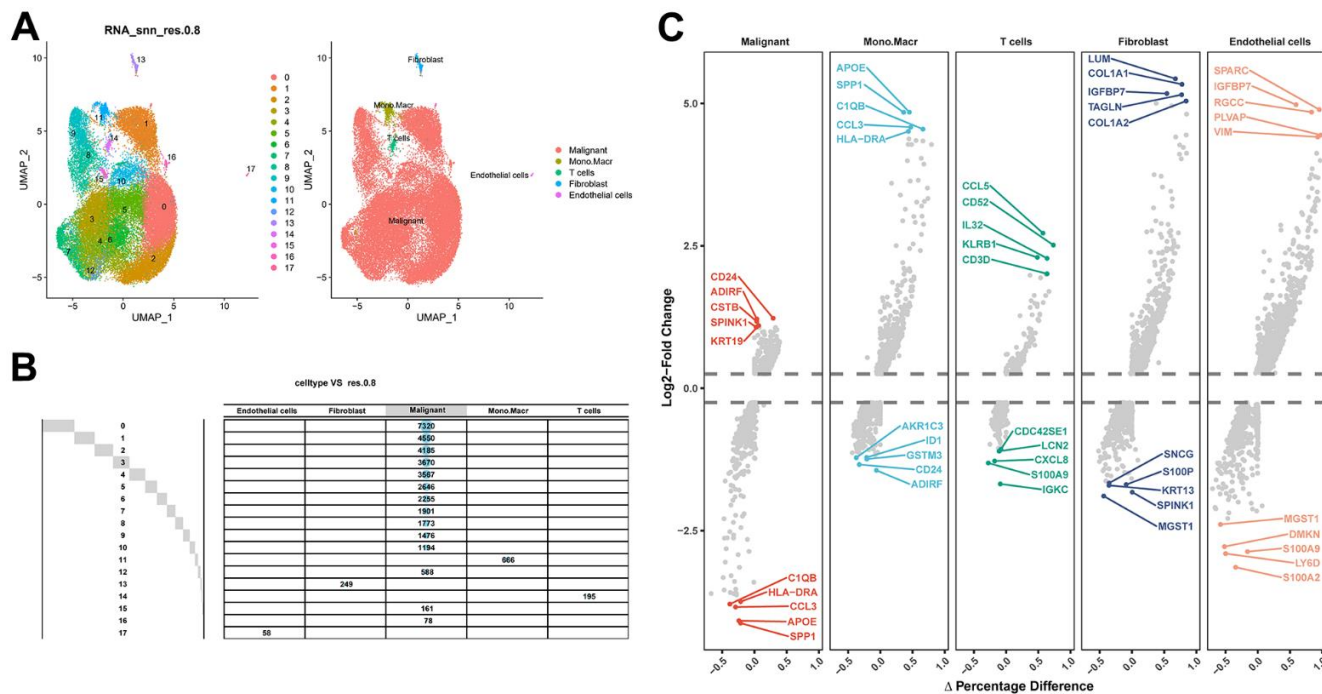

Figure 1. Identification of fibroblast marker genes based on scRNA-seq data. (**A**) 18 cell populations and 5 cell types visualized by the UMAP algorithm. (**B**) Amount of cells and attribution of each cell type. (**C**) Identification of top 5 differential genes for each cell type by FindAllMarkers.

differential genes is provided in Supplementary Table 2. Among the fibroblast marker genes, we selected the top 10 differentially expressed genes, namely LUM, COL1A1, IGFBP7, TAGLN, COL1A2, CXCL14, ACTA2, SPARC, COL3A1, and DCN, and visualized their expression patterns in cells using "FeaturePlot" (Figure 2). Additionally, we observed a positive correlation between these marker genes (p<0.0001), and the results of univariate regression analysis revealed that all nine marker genes, except for CXCL14, were prognostic risk factors (Figure 3B). Following batch effect removal, the TCGA-BLCA and GSE13507 datasets were combined as the testing set, which comprised 17147 genes and 576 samples (Figure 3A). The testing set was divided into gene high- and low-expression groups according to the best cutoff value, and our analysis demonstrated that the OS of BLCA patients was significantly worse (p<0.05) in the high-expression group of the majority of marker genes (Figure 3C).

Correlation between fibroblast marker gene subtypes and tumor immune microenvironment

Consensus clustering analysis revealed the presence of three subtypes based on the expression levels of marker genes (Figure 4A). Kaplan-Meier survival analysis demonstrated that the median OS of patients in cluster B was substantially lower than the other two subtypes (p=0.018) (Figure 4B). Figure 4C shows the comparison of gene expression levels among the three subtypes,

where cluster B had the highest expression levels of all marker genes, followed by cluster A (p<0.001). The distribution of the remaining clinical features in the three subtypes is shown in Figure 4D. We further performed pathway enrichment analysis for each subtype and found that cluster B was mainly enriched in immune, metabolic, and tumorigenesis-related pathways (Figure 5A–5C). Afterwards, we investigated the correlation between each subtype and the immune microenvironment by using the ESTIMATE algorithm. The results revealed that the stromal score, immune score, and estimated score of cluster B exhibited significantly higher values than those of the other two groups. (p<0.001) (Figure 6A, 6B). The results of the ssGSEA algorithm were similar and indicated that the infiltration level of most immune cells was higher in cluster B, with Monocyte, Myeloid-derived suppressor cells (MDSC), and T cells being the major immune cell types (Figure 6C).

Development of molecular subtypes and prognostic signature

A total of 723 DEGs were identified through a conjunction set following differential analysis among the subtypes (Figure 7A). Subsequently, GO/KEGG enrichment analysis revealed their association with an extracellular matrix structure, leukocyte migration, PI3K-Akt signaling pathway, and other functions (Figure 7B–7D). To detect prognosis-related genes, we performed univariate regression analysis and selected
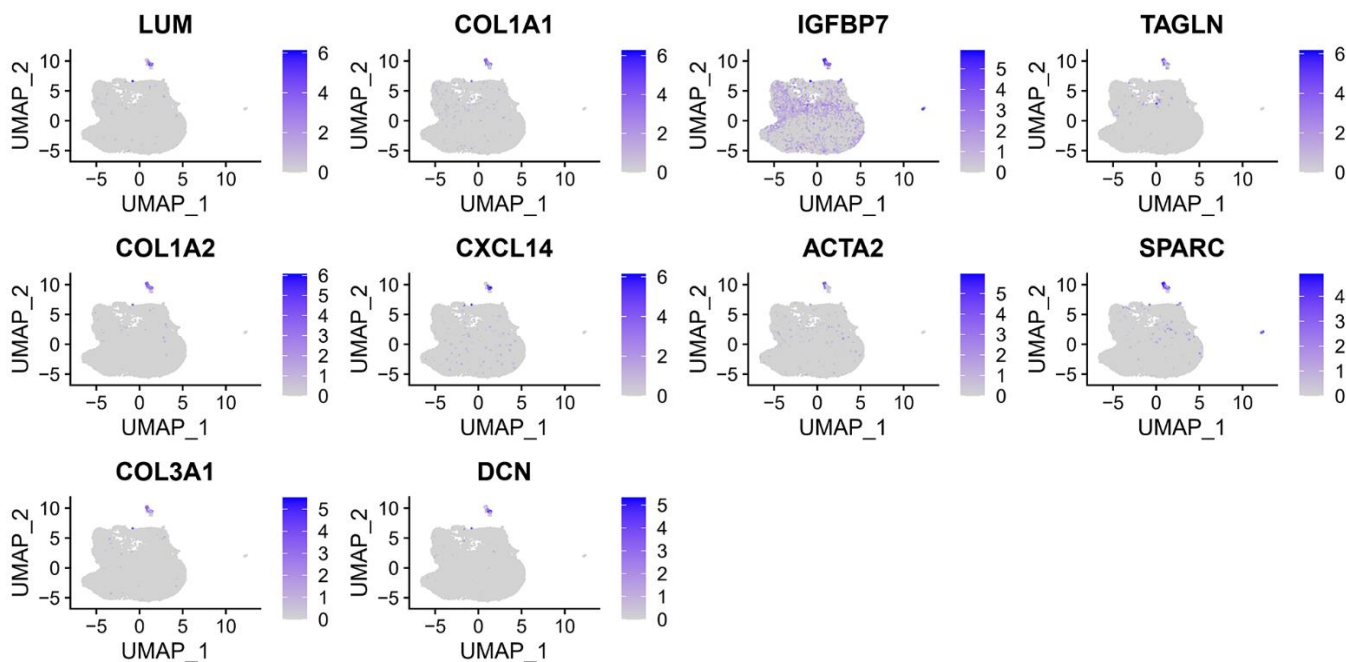

Figure 2. The expression of 10 fibroblast marker genes.

the top 10 genes with the smallest p-values as signature genes: EMP1, CERCAM, TM4SF1, FN1, HEYL, FBN1, ANXA1, LOX, SLC2A3, and SPOCD1. Among them, all but SPOCD1 were identified as prognostic risk factors (Figure 8A). Based on the signature genes, we classified the patients into two molecular subtypes (Figure 8B). Survival analysis revealed a significantly worse prognosis in patients belonging to gene cluster A (p<0.001) (Figure 8C), who also exhibited higher expression levels of signature genes (p<0.001). Furthermore, we compared the rest of the clinical

characteristics (Figure 8D, 8E). We established a prognostic signature to comprehensively capture the differences between the two molecular subtypes. We calculated the signature scores through GSVA and divided the testing set samples into high- and low-score groups based on the optimal cutoff value. The median OS of patients in the high-score group was significantly lower than that of the low-score group (p<0.001) (Figure 8F). In repeated subgroup analysis, we observed that all patients in the high-score group belonged to the gene cluster A subtype, while most patients in the
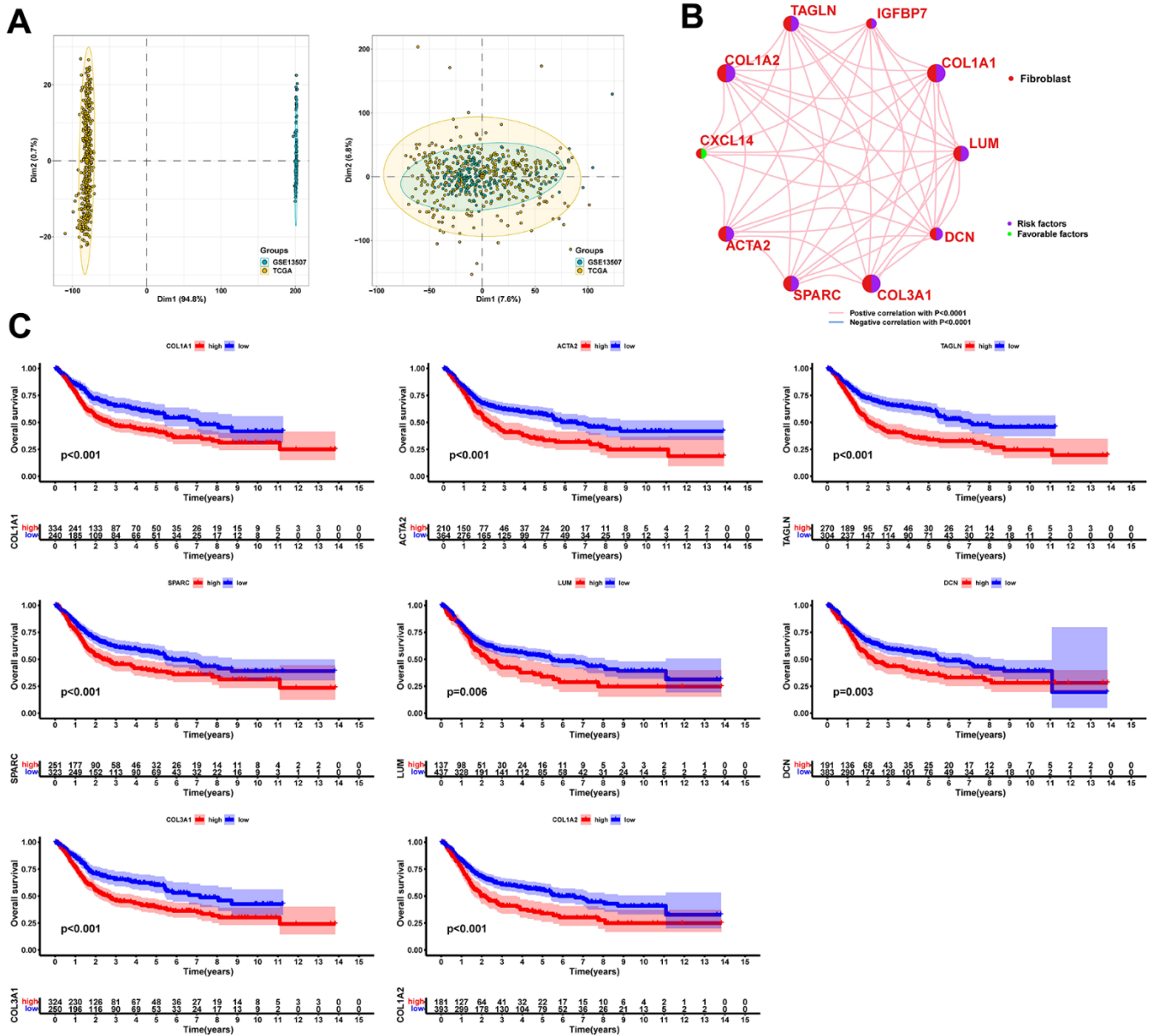
Figure 3. Significant correlation between fibroblast marker genes and prognosis of BLCA patients. (**A**) PCA plots of the testing set data before and after integration. (**B**) Correlation analysis and univariate regression analysis between fibroblast marker genes. Lines indicate a correlation between genes and p<0.0001; purple indicates a prognostic risk factor and green indicates a protective factor. (**C**) Kaplan-Meier curves for each marker gene with p<0.05.
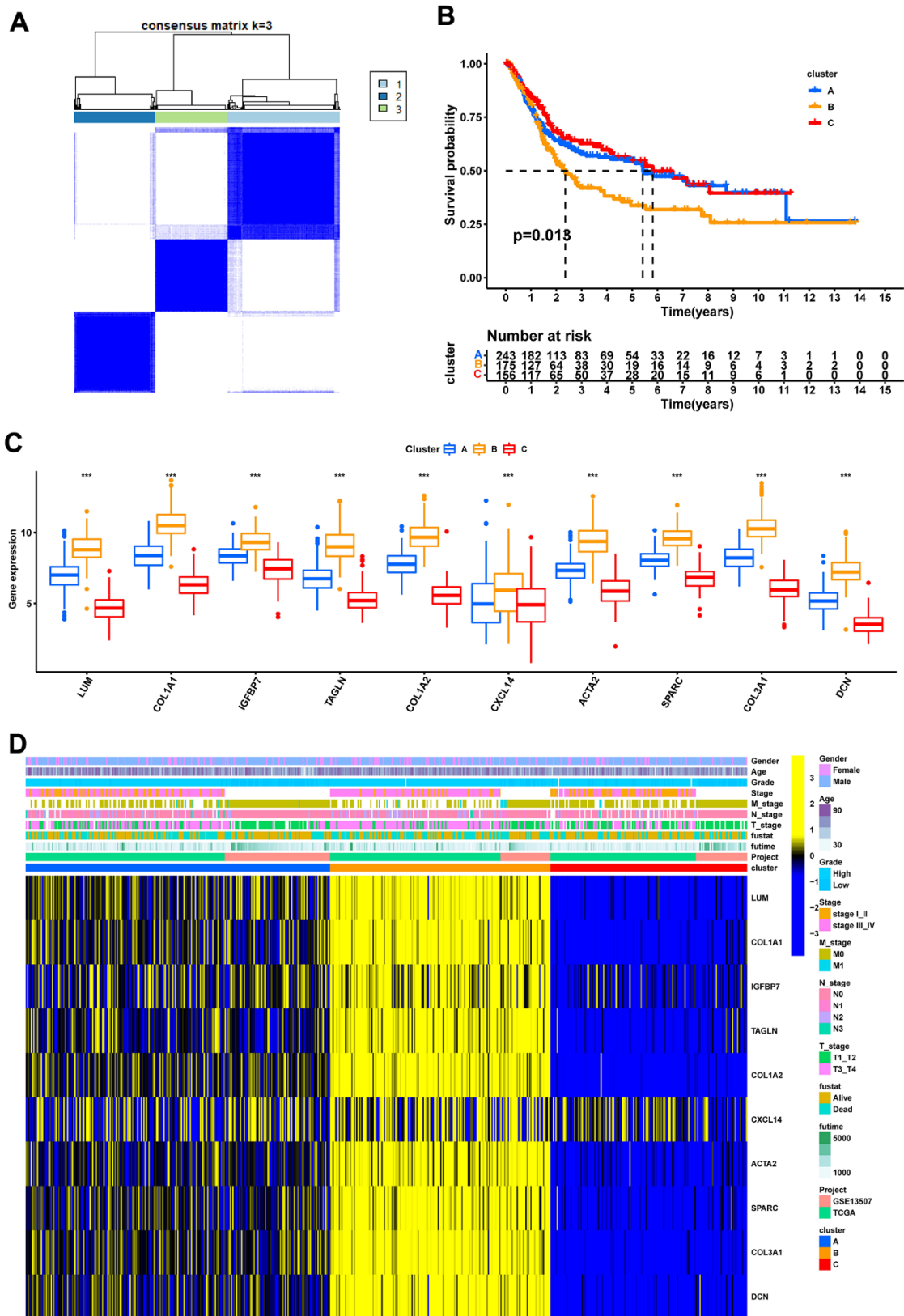
Figure 4. Recognition of 3 fibroblast marker gene subtypes by consensus clustering analysis. (**A**) Consensus matrix plots. K = 3 was determined as the optimal clustering number. (**B**) Kaplan-Meier survival analysis in clusters A, B, and C. (**C**) Differential expression of marker genes in fibroblast marker gene subtypes. (**D**) Heatmap of the marker gene expressions among clusters A, B, and C.

low-score group were in survival status. This indicates that the prognostic signature has good predictive value in BLCA (Figure 8G). Moreover, we found a significant positive correlation between risk score and multiple immune cell infiltrations (p<0.05), particularly MDSC, NKT cell, NK cell, and Treg cell (Figure 8H).

Validation of the risk score in different clinical patho-characteristic subgroups

The clinical characteristics of the tumor are of significant importance in determining its prognosis. Therefore, we evaluated the predictive capacity of the prognostic signature in patients exhibiting disparate states, genders, grades, N stages, T stages, and stages, by contrasting the discrepancies in clinical characteristics between high- and low-risk groups. Significant differences in risk scores were observed among all subgroups based on clinical characteristics, as illustrated in Figures 9A–9F. (p < 0.05). Moreover, the proportions of patients with death, high-grade, lymph node metastasis, T3/4, and stage III/IV were substantially higher in the high-score group than in

the low-score group. Hence, it is suggested that risk scores have excellent predictive potential for clinical outcomes.

Estimation and validation of the relationship between risk scores and immunotherapy response

Previous studies have reported that gene mutations can modify the response of cancer patients to immunotherapy and impact the selection of clinical drugs and treatment outcomes. Therefore, in this study, we compared gene mutation differences between the high- and low-score groups and found that missense mutation was the most common type of mutation in BLCA patients, and most genes were mutated more frequently in the high-score group (Supplementary Figure 2A–2C). We then analyzed the expression levels of cytokines and immune checkpoints in both groups. As shown in Figure 10A, most chemokines, interferons, and other cytokines, except interleukins, were notably over-expressed in the high-score group. The results of pathway enrichment analysis further confirmed that the risk score was positively correlated with tumorigenesis
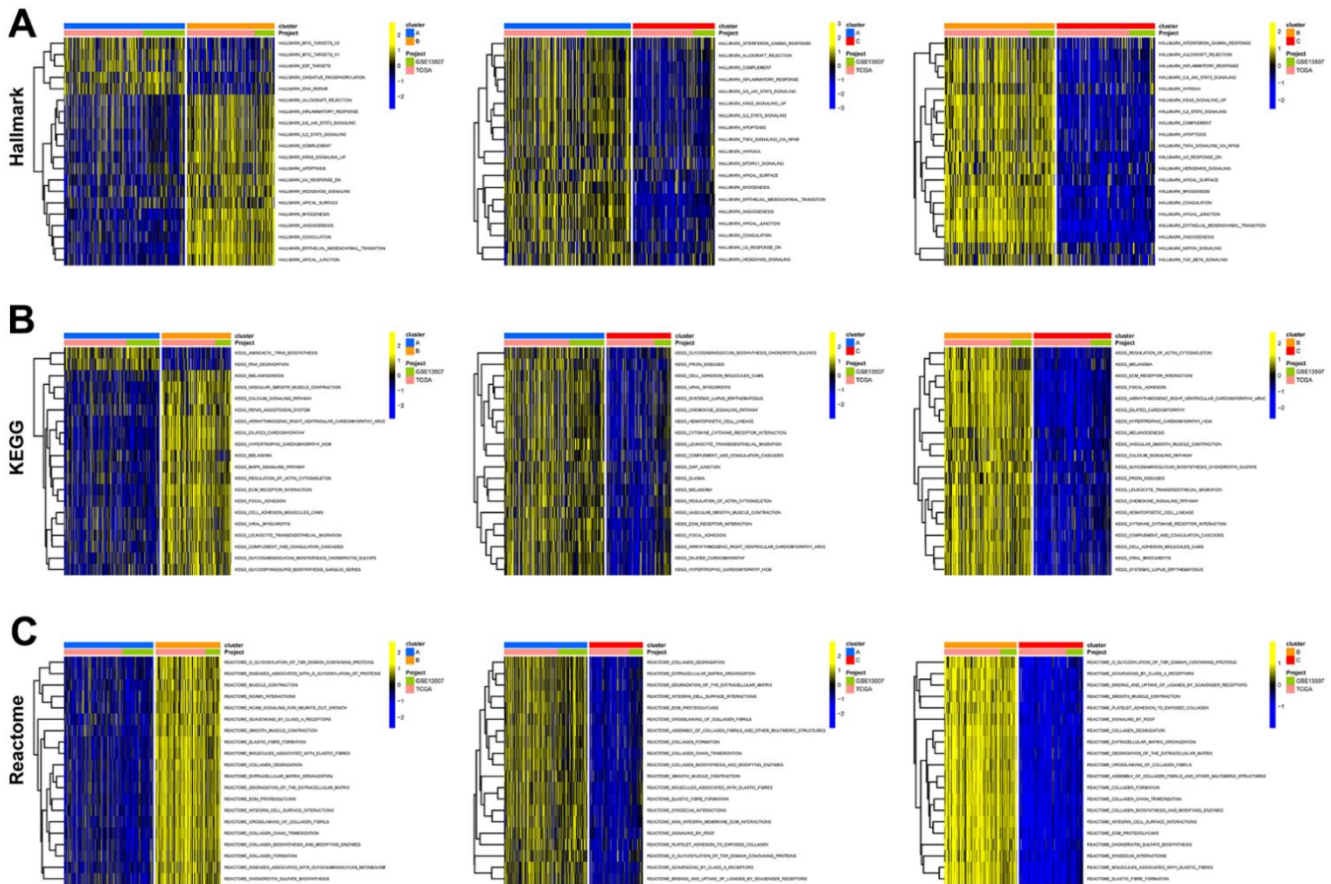

Figure 5. Functional enrichment analysis of fibroblast marker gene subtypes. (**A**) Enrichment analysis of 3 clusters in the HALLMARK pathway. (**B**) KEGG pathway. (**C**) Reactome pathway.

and multiple immune-related pathways, including EMT, angiogenesis, compliment, and IL-6/JAK/STAT3 signaling pathway (Figure 10B).

Similarly, our comparative analysis revealed that the expression levels of five immune checkpoints, LAG3, CD274, CTLA4, PDCD1, and TIGIT, were significantly elevated in the high-score group (p<0.001) (Figure 10C).

Collectively, these results demonstrated that the risk score was associated with the immunotherapy response in BLCA patients. To further substantiate this finding, we investigated the predictive value of the risk score by assigning patients in the GSE13507, GSE78220, and IMvigor210 cohorts to low-risk and high-risk groups. The risk score was found to have predictive value for immune checkpoint inhibitors. It was observed that
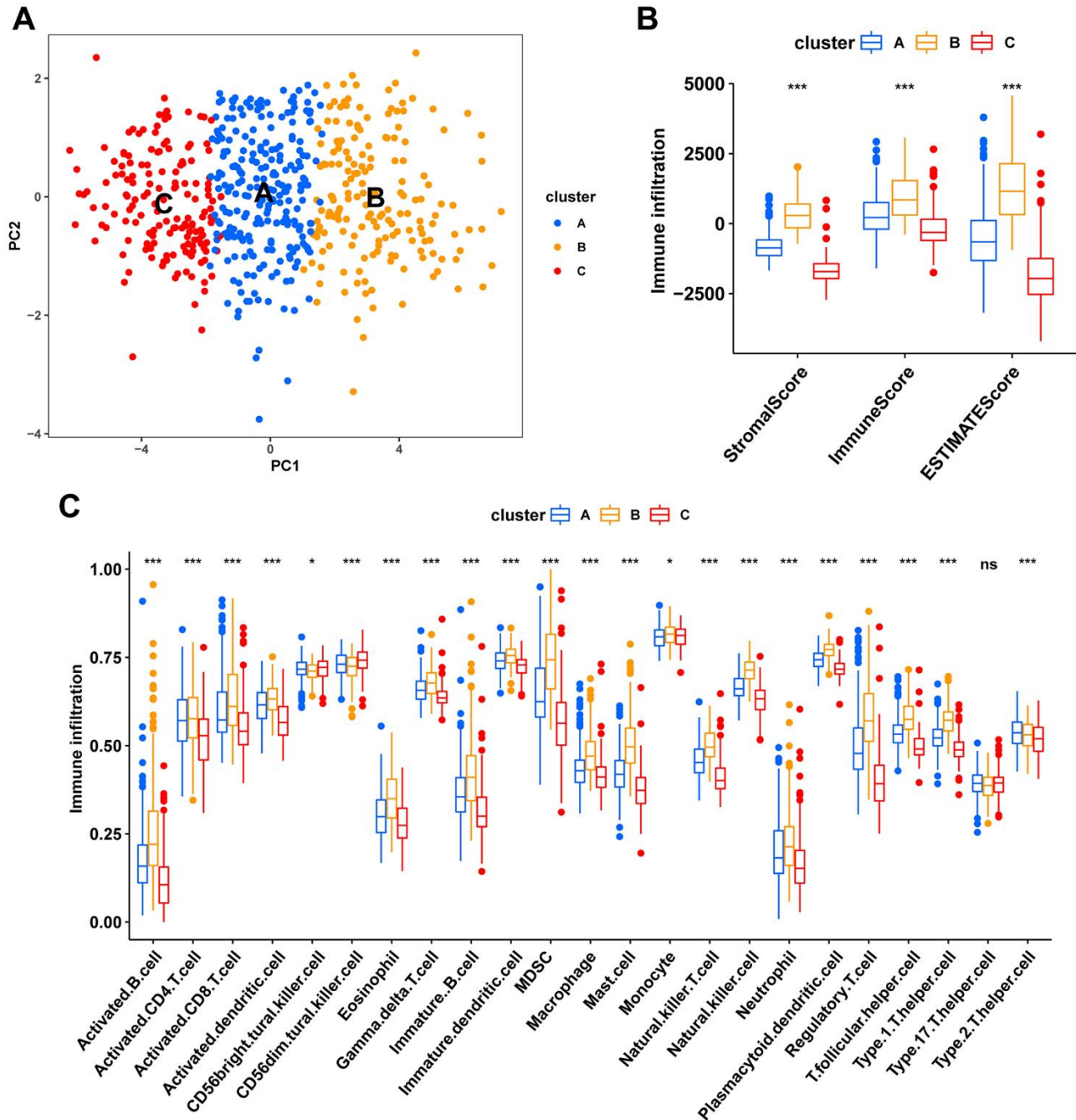
Figure 6. Characteristics of the tumor immune microenvironment in fibroblast marker gene subtypes. (**A**) PCA plots of the distribution of different subtype samples. (**B**) Differences in expression levels of stromal, immune, and ESTIMATE scores between clusters A, B, and C. (**C**) Differences in immune cell infiltration among different fibroblast marker gene subtypes.

patients who responded to anti-PD1, anti-PDL1, and intravesical BCG immunotherapy had distinctly lower risk scores. In contrast, patients in the high-score group had significantly worse objective response rates to immunotherapy and were more inclined to poorer survival outcomes ($p < 0.05$). Additionally, we found that patients with high-score had a higher incidence of tumor progression compared to patients with low-score (Figure 11A–11C). Taken together, these findings strongly suggest that the risk score may serve as a promising marker for immunotherapy in BLCA patients, potentially determining a specific immune profile. Patients in the high-score group are more likely to tolerate immunotherapy.

Prediction of potential sensitive drugs

Lastly, we investigated potentially sensitive chemotherapeutic agents for immunotherapy-tolerant patients. By comparing IC_{50} levels of chemotherapy drugs between the two groups, we found that patients in the low-score group exhibited lower IC_{50} values for anti-cancer drugs, including BIRB.0796, A.443654, ABT.888, AKT.inhibitor.VIII, ATRA, and BIBW2992. Patients with high scores were more likely to be sensitive to chemotherapy drugs, including AUY922, A.770041, AG.014699, AICAR, AMG.706, and AP.24534 (Figure 12).

Validation of genes using IHC and *in vitro* assays

The RT-qPCR results revealed a statistically significant difference in gene expression between normal bladder uroepithelial cells and BLCA for the nine genes analyzed (Supplementary Figure 3). Furthermore, the expression patterns of most genes observed in the PCR experiments were consistent with those observed in TCGA transcriptome data. To validate these experimental results at the translational level, IHC experiments were performed (Supplementary Figure 4). The expression levels of the nine genes were found to be consistent between mRNA and protein levels.
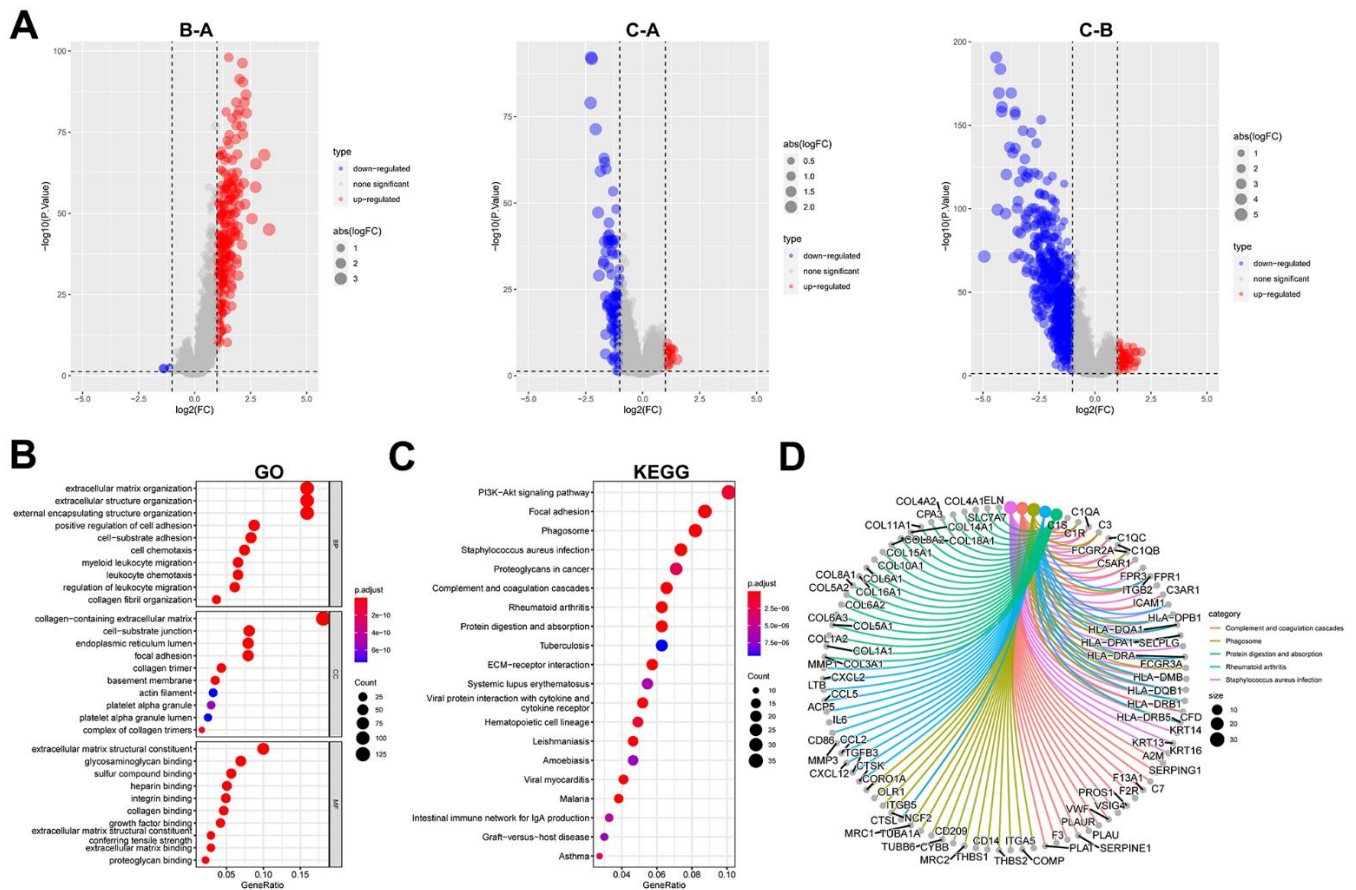

Figure 7. Identification and functional enrichment analysis of DEGs between fibroblast marker gene subtypes. (**A**) Volcano plots of differential expression of genes among clusters A, B, and C. The red dots represent upregulated genes and the blue dots represent downregulated genes. (**B**) Bubble plots of the GO terms of differential expression of genes. (**C**) Bubble plots of the KEGG pathways of differential expression of genes. (**D**) Correspondence between top 5 pathway and genes in KEGG.

DISCUSSION

Despite extensive use in tumor patients, immuno-therapy's response rate is not as excellent as expected. One of the most influential factors in the occurrence of immunotherapy resistance is the tumor immune escape mechanism. Evidence suggests that antigen-presenting cells are crucial for T-cell activation and tumor immunity, and cancers can evade this immunity through immune editing mechanisms such as immune dominance, the absence of immune checkpoints, or downregulating antigen-presenting cells. Recent advancements in cancer research have highlighted the TME as a key determinant of patients' responses to immunotherapy [30–32]. CAFs, essential components

of the TME, regulate tumor proliferation, angiogenesis, invasion, metastasis, and treatment resistance in numerous malignancies. The application of scRNA-seq technology has revealed the molecular features and heterogeneity of various cell types within the TME, primarily focusing on immune cells [33, 34]. However, the investigation of stromal cells within the TME has been limited. Fibroblasts, which constitute the majority of stromal cells in the TME, play a vital role in anti-tumor immunity. At the initial stages of malignancy, fibroblasts can secrete TGFβ and hepatocyte growth factor, inducing the initiation of cancer within the normal human epithelium. Therefore, we employed a combination of bulk RNA-seq and scRNA-seq analyses to identify fibroblast-specific marker genes.
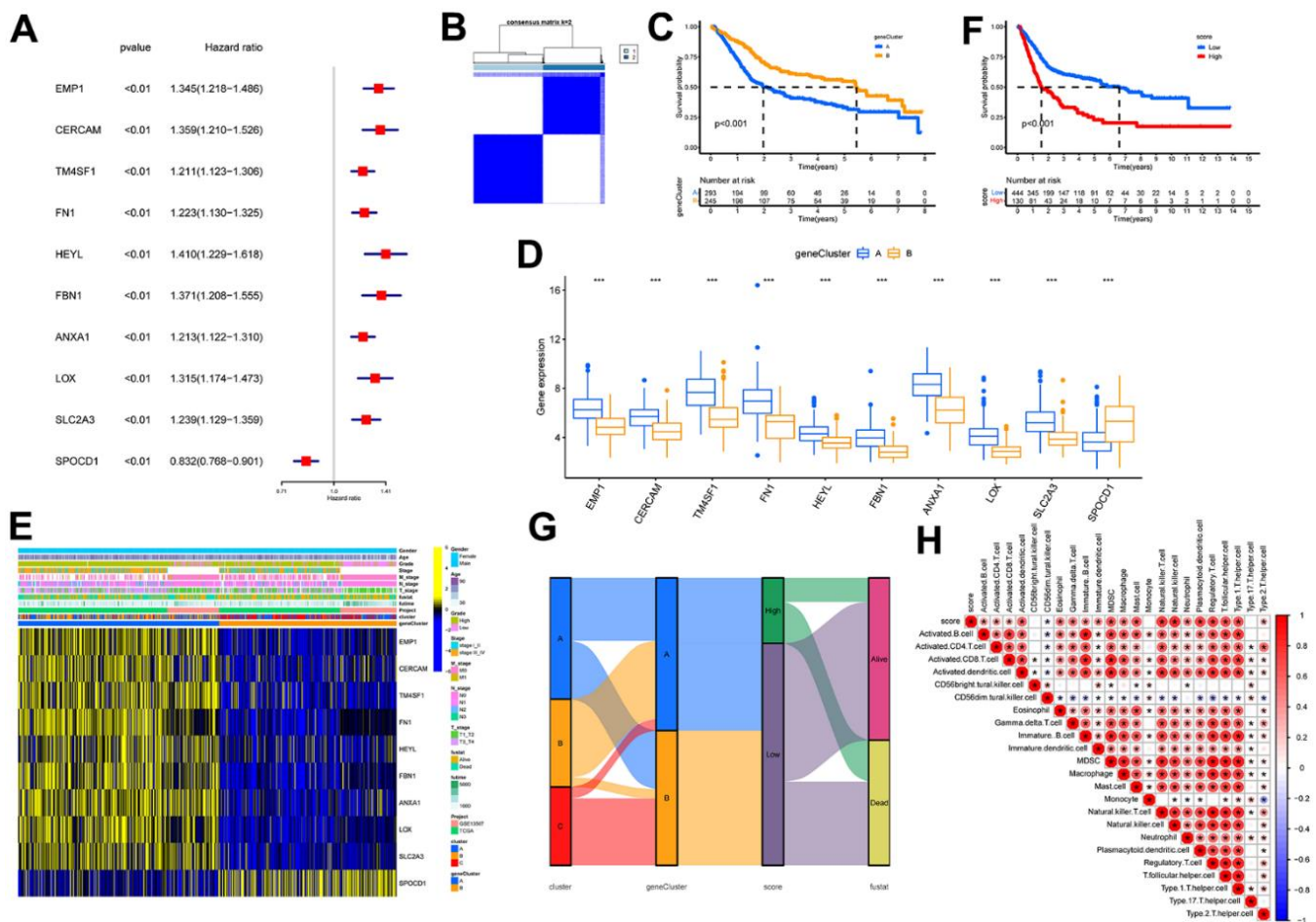

Figure 8. Identification of molecular subtypes and prognostic signature. (**A**) Forest plots for the univariate regression analysis of the 10 signature genes. (**B**) Consensus matrix plots based on signature genes. K = 2 was determined as the optimal clustering number. (**C**) Kaplan-Meier survival analysis in molecular subtypes A and B. Patients in subtypes A were related to a poorer prognosis than those in subtypes B. (**D**) Differential expression of signature genes in molecular subtypes. *** indicates p<0.001. (**E**) Heatmap of the signature gene expressions among molecular subtypes A and B. (**F**) Kaplan-Meier survival analysis between high- and low-score groups. Patients in high-score groups were related to a poorer prognosis compared to those in low-score groups. (**G**) Sankey diagram showing the dynamics of individual clusters concerning survival status. (**H**) Heat map of the correlation between prognostic signature score and immune cell infiltration. Red represents a positive correlation, blue represents a negative correlation; * indicates p<0.05.

Subsequently, we classified BLCA patients into three distinct molecular subtypes using these markers and developed and validated a prognostic signature to predict the survival outcome and responsiveness to immunotherapy in these patients.

Our findings demonstrate that the fibroblast-related prognostic signature is significantly associated with clinical characteristics and outcomes of BLCA patients. The high-score group was characterized by a higher grade, a more advanced stage, and an inferior OS. These results are consistent with previous studies that have linked fibroblast activity to poor cancer prognosis, but our study uniquely identifies specific marker genes and their implications in BLCA. Furthermore, the signature was validated across multiple datasets, demonstrating good stability in predicting OS. This prompted us to investigate the underlying mechanisms in greater depth. We determined ten genes (EMP1, CERCAM, TM4SF1, FN1, HEYL, FBN1, ANXA1, LOX, SLC2A3, and
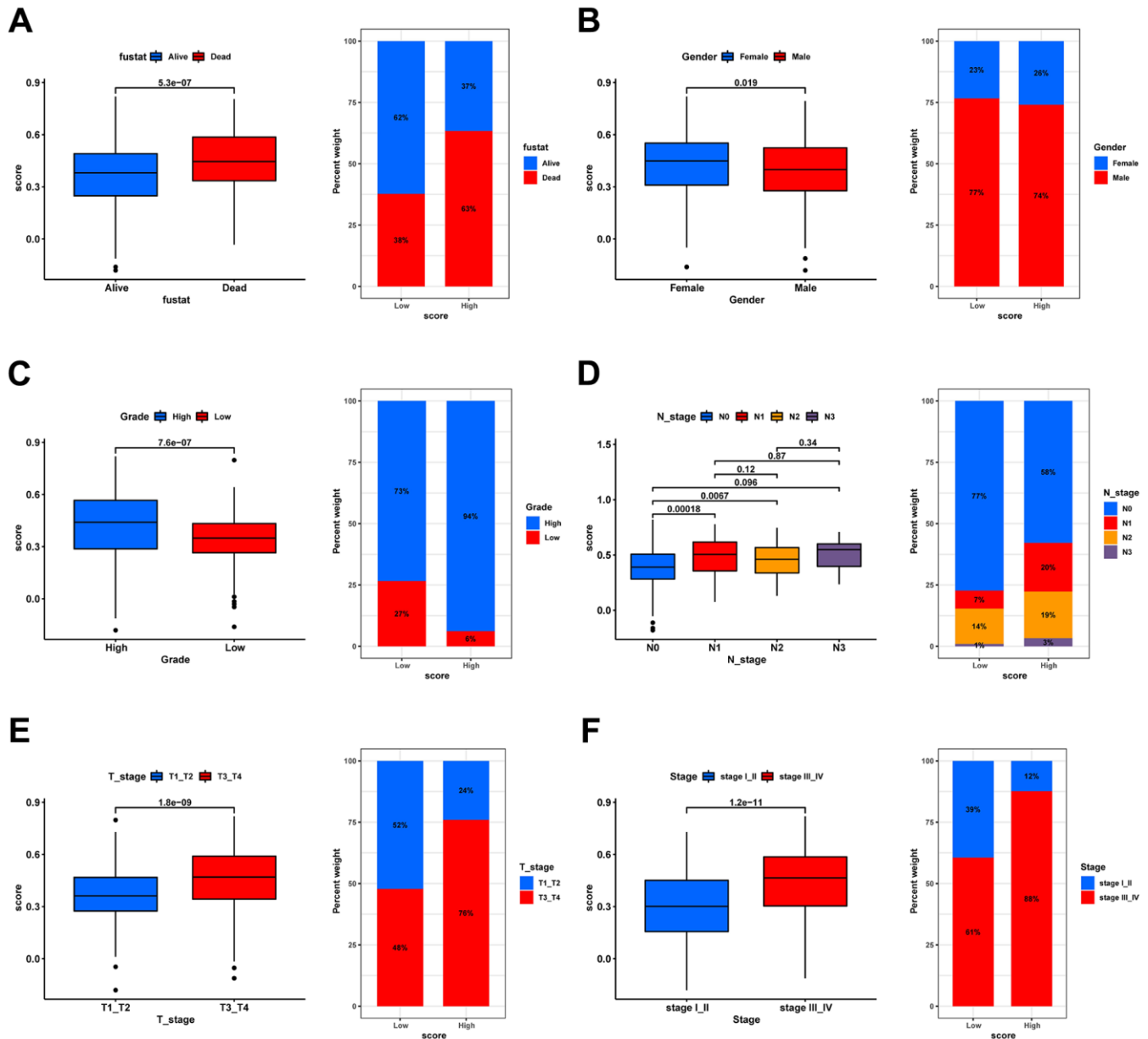
Figure 9. Correlation analysis of risk scores with clinical characteristics. Box plot for differences in risk score distribution (left) and bar plot for sample distribution in high- and low-risk groups (right) in different survival status (A), gender (B), grade (C), N stage (D), T stage (E), and tumor stage (F).

SPOCD1) that constituted the prognostic signature. HEYL, SLC2A3, and FBN1 were found to mediate tumor progression and chemoresistance mainly by facilitating angiogenesis and EMT [35–37], while CERCAM, ANXA1, and SPOCD1 promoted tumor progression through the PI3K/AKT and EGFR signaling pathways. The remaining genes were associated with immune cell infiltration and immunotherapeutic response [38–40]. After conducting GSVA analysis, we hypothesized that certain genes might contribute to the poorer prognosis observed in the high-score group. Additionally, studies have shown that OICR-9429 enhances the chemosensitivity of bladder cancer cells to cisplatin, increasing apoptosis rates and cisplatin cytotoxicity, thus holding significant clinical implications [41]. Remodelin, by inhibiting NAT10 expression, has been found to increase bladder cancer patients' sensitivity to cisplatin, reducing the S phase population in the cell cycle, enhancing bladder cancer cell chemosensitivity to cisplatin, and inducing apoptosis [42]. This underscores the importance of discovering novel targets for chemoresistance in bladder cancer, representing a promising avenue of research.

Our comprehensive investigation into the relationship between the prognostic signature and the tumor immune microenvironment revealed a positive correlation between the risk score and the infiltration of multiple immune cells, including MDSC, NK cells, and Treg cells. While cytotoxic T cells are critical effector molecules in anti-tumor immunity, CAFs and Treg cells can create immunologic barriers that lead to cytotoxic T cell dysfunction or exhaustion during cancer progression [43, 44]. This suggests that patients in the high-score group may experience reduced anti-tumor activity.
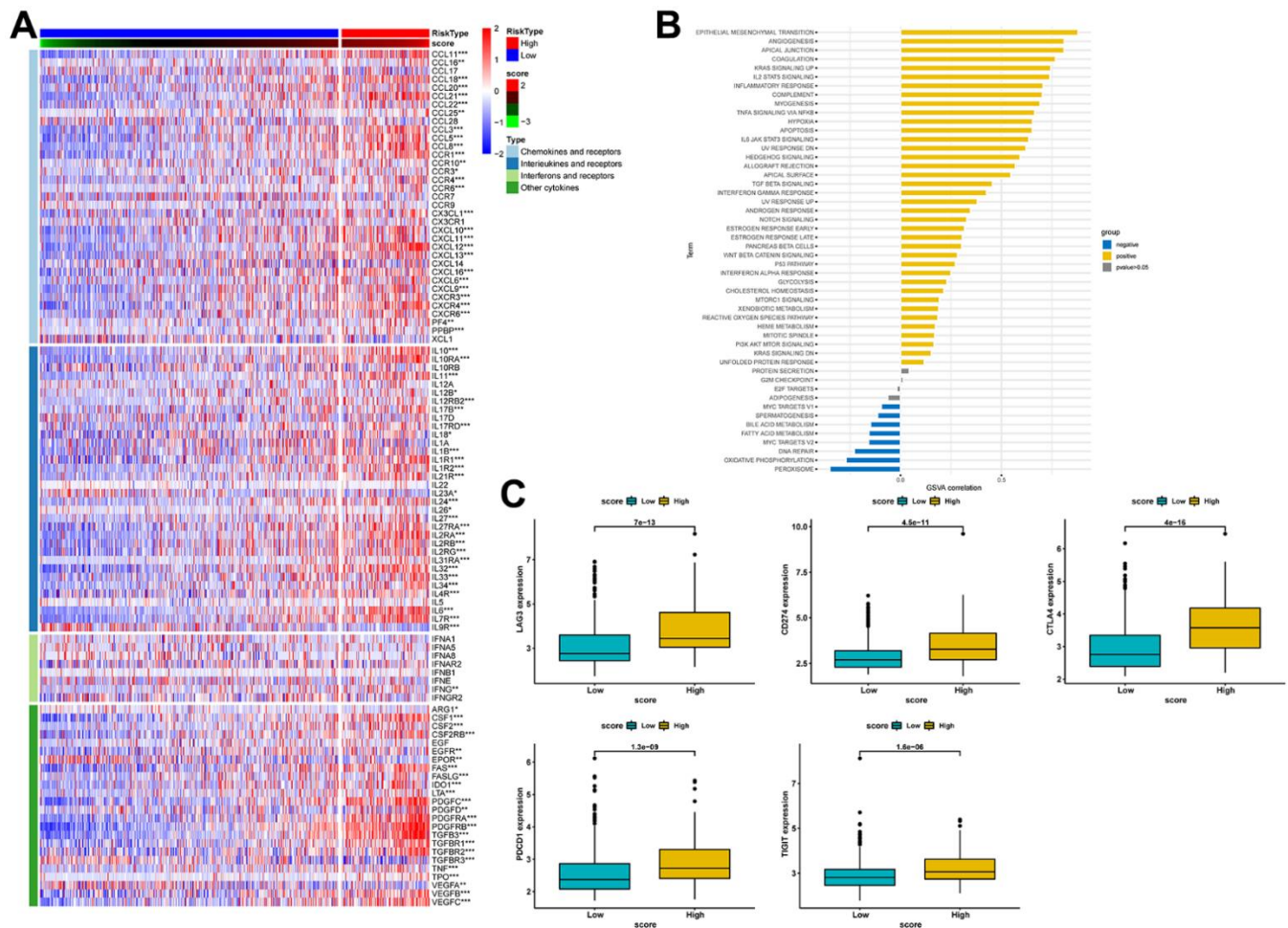

Figure 10. Estimation of the relationship between risk scores and the tumor immune microenvironment. (A) Heat map of cytokine expression in high- and low-score groups. * indicates p<0.05, ** indicates p<0.01, *** indicates p<0.001. (B) Correlations between signature score and HALLMARK pathway. (C) Expression analysis of LAG3, CD274, CTLA-4, PDCD1, and TIGIT between high- and low-risk groups.

Further analysis showed that patients in the high-score group had significantly elevated levels of chemokine expression. The role of chemokines in the tumor immune response is bidirectional. Pro-tumorigenic immune cells can recruit immunosuppressive cells via chemokine-dependent infiltration at different tumorigenesis stages and immune cell activation states, thereby reinforcing pro-tumorigenic responses [45]. This
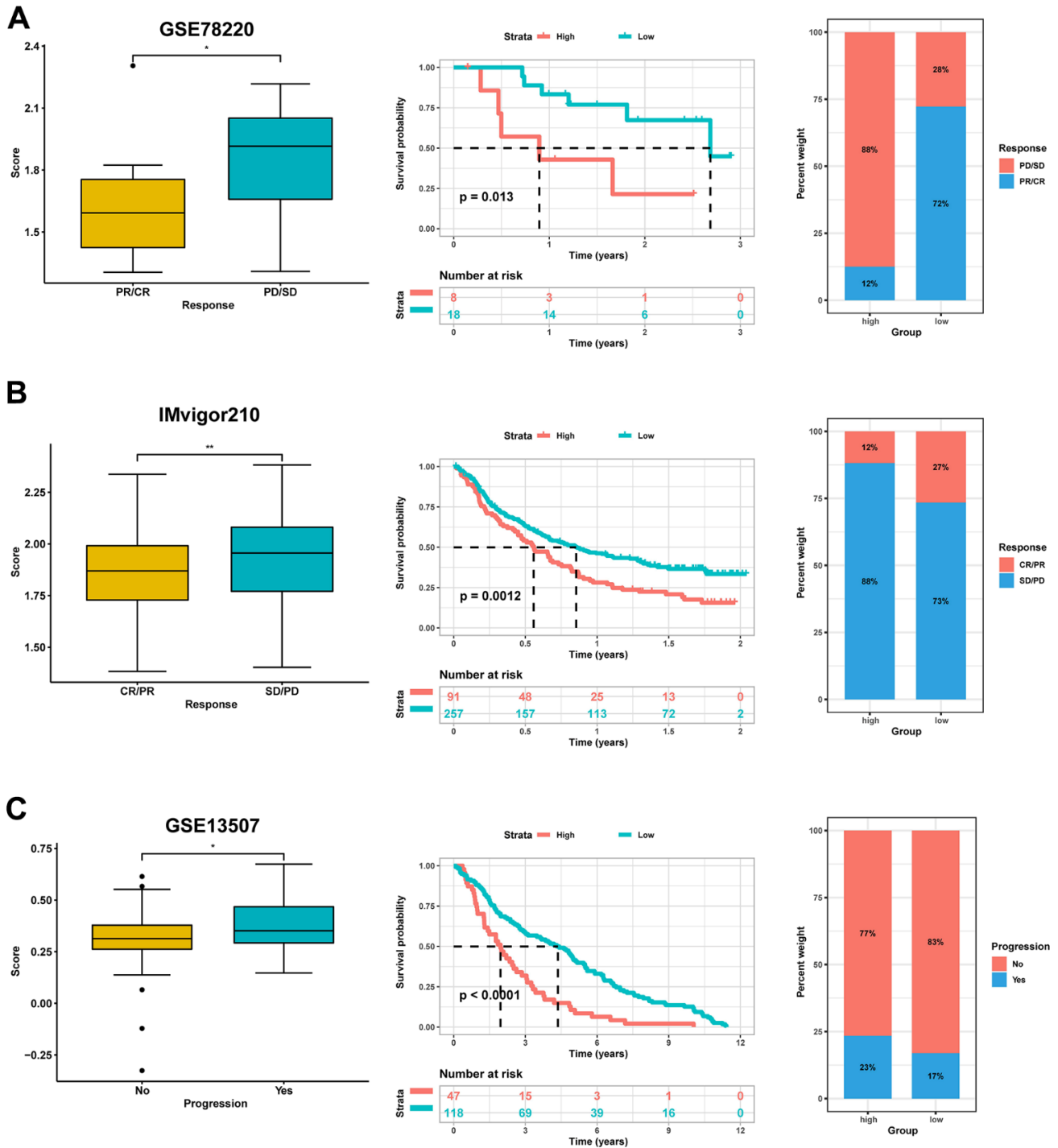

Figure 11. Validation for the predictive role of risk score on the immunotherapeutic response. (**A**) Kaplan-Meier survival analysis and distribution of immunotherapy responses of high- and low-score groups in GSE78220. (**B**) Kaplan-Meier survival analysis and distribution of immunotherapy responses of high- and low-score groups in IMvigor210 dataset. (**C**) Kaplan-Meier survival analysis and progress risk of high- and low-score groups in the GSE13507 dataset.

phenomenon may partially contribute to the observed immunosuppression in the high-score group.

Immune checkpoint molecules are crucial for immune function and have significant clinical implications in immunotherapy. Motivated by discrepancies in the tumor immune microenvironment, we explored the potential of the prognostic signature to predict responses to immunotherapy. We observed that patients in the high-score group had elevated levels of immune
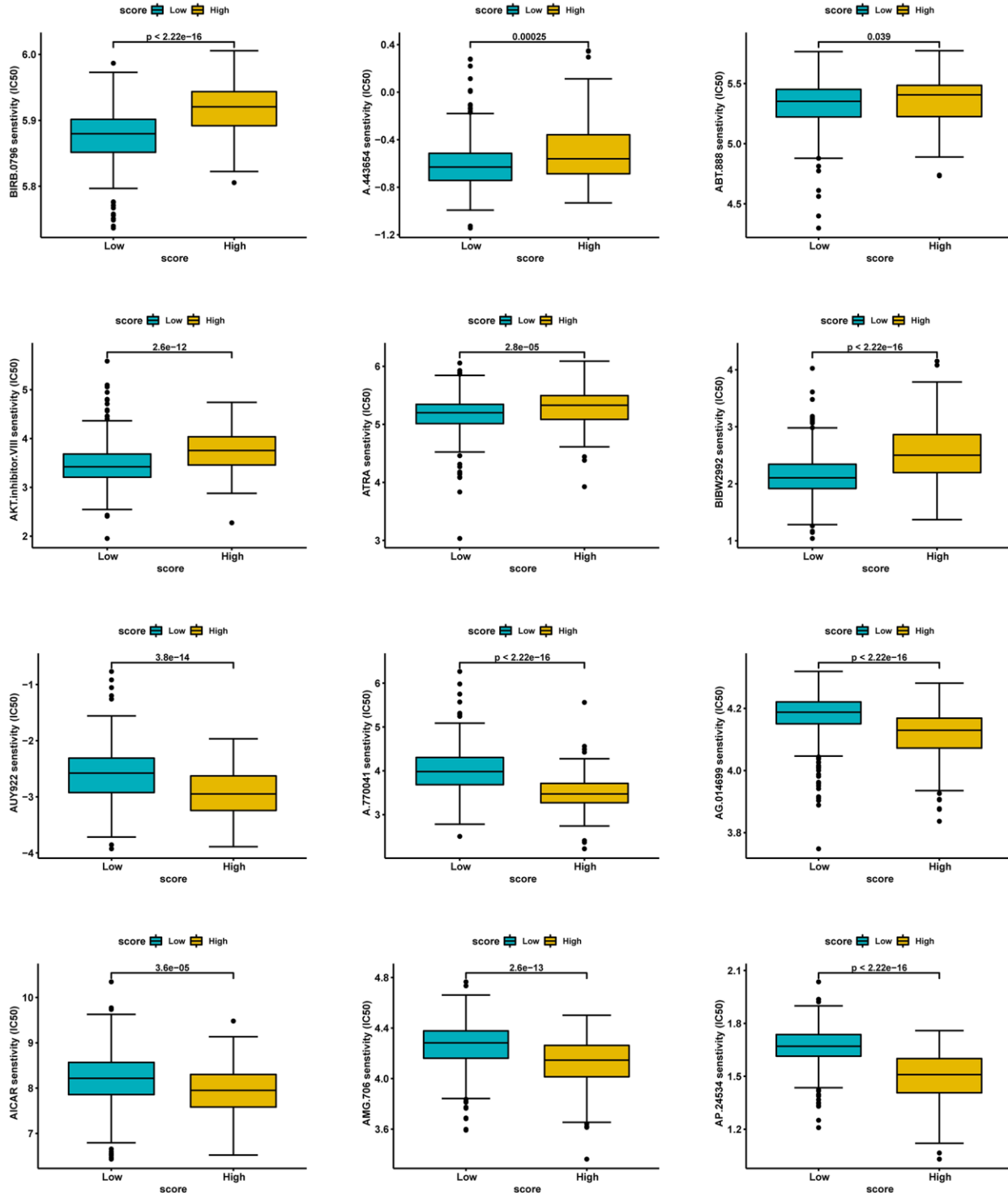

Figure 12. Prediction of potential sensitive drugs in high- and low-score groups.

checkpoints but exhibited poorer response rates to immunotherapy. These findings suggest immune exhaustion as a possible mechanism behind the resistance to immunotherapy in the high-score group. This is particularly innovative, as it indicates specific molecular targets for overcoming immune resistance in BLCA patients.

The purpose of the signature is to enhance patients' responses to immunotherapy and to identify methods of overcoming immune resistance. We predicted potential target drugs and found that both high- and low-scoring groups might benefit from six different anti-tumor drugs, including VEGFR inhibitors, AMPK activators, and PARP inhibitors, among others. For instance, Li et al. found that VEGFR and EGFR inhibition increases epithelial characteristics and chemotherapy sensitivity in mesenchymal bladder cancer cells [46]. Zhou et al. revealed that artesunate induces autophagy-dependent apoptosis through up-regulating ROS and activating AMPK-mTOR-ULK1 axis in human bladder cancer cells [47]. Moreover, Bhattacharjee et al. discovered that PARP inhibitors enhance and synergize with cisplatin to inhibit bladder cancer cell survival and tumor growth [48]. Collectively, these findings could serve as a clinical reference for selecting drugs, although these drugs need further confirmation through clinical studies before they can be applied.

The present study has some limitations that can be addressed in future work. Firstly, we constructed the prognostic signature using the ten most relevant prognostic genes, but other prognostic-related genes were not included, which may introduce some bias. To avoid selection bias and enhance the accuracy of the analysis, future validation of this signature will require more prospective and multicenter BLCA cohorts. Secondly, the sample size of scRNA-seq data is relatively small, and clinicopathological characteristic data were unavailable. Bulk RNA-seq analysis of a larger sample size partially compensates for this limitation and ensures the accuracy of the prognostic signature. Thirdly, it should be noted that the mechanisms discussed in this study and the sensitive drug predictions are primarily based on the analysis of public databases and theoretical descriptions. Further *in vivo* and *in vitro* experiments are required to confirm the predictive value and potential mechanisms of this signature. Lastly, biomarker-driven prospective clinical trials are needed to determine treatment decisions for advanced-stage tumors. Therefore, our next objective is to conduct a comprehensive study aimed at elucidating the potential mechanisms underlying this signature, with the ultimate goal of its clinical application.

CONCLUSIONS

After analyzing scRNA-seq and bulk RNA-seq data, we have successfully developed and validated a risk signature associated with fibroblasts. This signature can serve as an independent prognostic indicator for patients diagnosed with BLCA. The signature is reliable and robust and can accurately predict the outcomes for BLCA patients. This can help clinicians make more informed and rational decisions related to treatment.

AUTHOR CONTRIBUTIONS

JW, ZT and HL contributed to the study's inception and design. JW and CL performed bioinformatics analyses and assisted with the analysis of other data. ZT, YH and PZ performed the experiments. HW and HL helped to revise the manuscript. All authors have read and approved the final manuscript.

ACKNOWLEDGMENTS

CONFLICTS OF INTEREST

The authors declare that they have no conflicts of interest.

ETHICAL STATEMENT AND CONSENT

This study was approved by the ethics committee of The Second Affiliated Hospital of Kunming Medical University (Approval Number: KYD213238) and carried out under the World Medical Association Declaration of Helsinki. All patients provided written informed consent before their inclusion in the study.

FUNDING

REFERENCES

1. Damrauer JS, Beckabir W, Klomp J, Zhou M, Plimack ER, Galsky MD, Grivas P, Hahn NM, O'Donnell PH, Iyer

G, Quinn DI, Vincent BG, Quale DZ, et al. Collaborative study from the Bladder Cancer Advocacy Network for the genomic analysis of metastatic urothelial cancer. Nat Commun. 2022; 13:6658. https://doi.org/10.1038/s41467-022-33980-9 PMID:36333289

2. Sung H, Ferlay J, Siegel RL, Laversanne M, Soerjomataram I, Jemal A, Bray F. Global Cancer Statistics 2020: GLOBOCAN Estimates of Incidence and Mortality Worldwide for 36 Cancers in 185 Countries. CA Cancer J Clin. 2021; 71:209–49. https://doi.org/10.3322/caac.21660 PMID:33538338

3. Witjes JA, Bruins HM, Cathomas R, Compérat EM, Cowan NC, Gakis G, Hernández V, Linares Espinós E, Lorch A, Neuzillet Y, Rouanne M, Thalmann GN, Veskimäe E, et al. European Association of Urology Guidelines on Muscle-invasive and Metastatic Bladder Cancer: Summary of the 2020 Guidelines. Eur Urol. 2021; 79:82–104. https://doi.org/10.1016/j.eururo.2020.03.055 PMID:32360052

4. Chen X, Xie R, Gu P, Huang M, Han J, Dong W, Xie W, Wang B, He W, Zhong G, Chen Z, Huang J, Lin T. Long Noncoding RNA *LBCS* Inhibits Self-Renewal and Chemoresistance of Bladder Cancer Stem Cells through Epigenetic Silencing of SOX2. Clin Cancer Res. 2019; 25:1389–403. https://doi.org/10.1158/1078-0432.CCR-18-1656 PMID:30397178

5. Liu S, Chen X, Lin T. Emerging strategies for the improvement of chemotherapy in bladder cancer: Current knowledge and future perspectives. J Adv Res. 2022; 39:187–202. https://doi.org/10.1016/j.jare.2021.11.010 PMID:35777908

6. Patel VG, Oh WK, Galsky MD. Treatment of muscle-invasive and advanced bladder cancer in 2020. CA Cancer J Clin. 2020; 70:404–23. https://doi.org/10.3322/caac.21631 PMID:32767764

7. Balar AV. Immune Checkpoint Blockade in Metastatic Urothelial Cancer. J Clin Oncol. 2017; 35:2109–12. https://doi.org/10.1200/JCO.2017.72.8444 PMID:28481707

8. Zou W, Wolchok JD, Chen L. PD-L1 (B7-H1) and PD-1 pathway blockade for cancer therapy: Mechanisms, response biomarkers, and combinations. Sci Transl Med. 2016; 8:328rv4. https://doi.org/10.1126/scitranslmed.aad7118 PMID:26936508

9. Sonpavde G, Dranitsaris G, Necchi A. Improving the Cost Efficiency of PD-1/PD-L1 Inhibitors for Advanced Urothelial Carcinoma: A Major Role for Precision Medicine? Eur Urol. 2018; 74:63–5. https://doi.org/10.1016/j.eururo.2018.03.015 PMID:29653886

10. Hanahan D, Coussens LM. Accessories to the crime: functions of cells recruited to the tumor microenvironment. Cancer Cell. 2012; 21:309–22. https://doi.org/10.1016/j.ccr.2012.02.022 PMID:22439926

11. Bahcecioglu G, Basara G, Ellis BW, Ren X, Zorlutuna P. Breast cancer models: Engineering the tumor microenvironment. Acta Biomater. 2020; 106:1–21. https://doi.org/10.1016/j.actbio.2020.02.006 PMID:32045679

12. Tiwari A, Trivedi R, Lin SY. Tumor microenvironment: barrier or opportunity towards effective cancer therapy. J Biomed Sci. 2022; 29:83. https://doi.org/10.1186/s12929-022-00866-3 PMID:36253762

13. Ringuette Goulet C, Bernard G, Tremblay S, Chabaud S, Bolduc S, Pouliot F. Exosomes Induce Fibroblast Differentiation into Cancer-Associated Fibroblasts through TGFβ Signaling. Mol Cancer Res. 2018; 16:1196–204. https://doi.org/10.1158/1541-7786.MCR-17-0784 PMID:29636362

14. Mhaidly R, Mechta-Grigoriou F. Fibroblast heterogeneity in tumor micro-environment: Role in immunosuppression and new therapies. Semin Immunol. 2020; 48:101417. https://doi.org/10.1016/j.smim.2020.101417 PMID:33077325

15. Costa A, Kieffer Y, Scholer-Dahirel A, Pelon F, Bourachot B, Cardon M, Sirven P, Magagna I, Fuhrmann L, Bernard C, Bonneau C, Kondratova M, Kuperstein I, et al. Fibroblast Heterogeneity and Immunosuppressive Environment in Human Breast Cancer. Cancer Cell. 2018; 33:463–79.e10. https://doi.org/10.1016/j.ccell.2018.01.011 PMID:29455927

16. De Jaeghere EA, Denys HG, De Wever O. Fibroblasts Fuel Immune Escape in the Tumor Microenvironment. Trends Cancer. 2019; 5:704–23. https://doi.org/10.1016/j.trecan.2019.09.009 PMID:31735289

17. Burley A, Rullan A, Wilkins A. A review of the biology and therapeutic implications of cancer-associated fibroblasts (CAFs) in muscle-invasive bladder cancer. Front Oncol. 2022; 12:1000888. https://doi.org/10.3389/fonc.2022.1000888 PMID:36313650

18. Azizi E, Carr AJ, Plitas G, Cornish AE, Konopacki C, Prabhakaran S, Nainys J, Wu K, Kiseliovas V, Setty M, Choi K, Fromme RM, Dao P, et al. Single-Cell Map of Diverse Immune Phenotypes in the Breast Tumor Microenvironment. Cell. 2018; 174:1293–308.e36. https://doi.org/10.1016/j.cell.2018.05.060 PMID:29961579

19. Leek JT, Johnson WE, Parker HS, Jaffe AE, Storey JD. The sva package for removing batch effects and other unwanted variation in high-throughput experiments. Bioinformatics. 2012; 28:882–3. https://doi.org/10.1093/bioinformatics/bts034 PMID:22257669

20. Mariathasan S, Turley SJ, Nickles D, Castiglioni A, Yuen K, Wang Y, Kadel EE II, Koeppen H, Astarita JL, Cubas R, Jhunjhunwala S, Banchereau R, Yang Y, et al. TGFβ attenuates tumour response to PD-L1 blockade by contributing to exclusion of T cells. Nature. 2018; 554:544–8. https://doi.org/10.1038/nature25501 PMID:29443960

21. Gribov A, Sill M, Lück S, Rücker F, Döhner K, Bullinger L, Benner A, Unwin A. SEURAT: visual analytics for the integrated analysis of microarray data. BMC Med Genomics. 2010; 3:21. https://doi.org/10.1186/1755-8794-3-21 PMID:20525257

22. Becht E, McInnes L, Healy J, Dutertre CA, Kwok IWH, Ng LG, Ginhoux F, Newell EW. Dimensionality reduction for visualizing single-cell data using UMAP. Nat Biotechnol. 2018. [Epub ahead of print]. https://doi.org/10.1038/nbt.4314 PMID:30531897

23. Aran D, Looney AP, Liu L, Wu E, Fong V, Hsu A, Chak S, Naikawadi RP, Wolters PJ, Abate AR, Butte AJ, Bhattacharya M. Reference-based analysis of lung single-cell sequencing reveals a transitional profibrotic macrophage. Nat Immunol. 2019; 20:163–72. https://doi.org/10.1038/s41590-018-0276-y PMID:30643263

24. Wilkerson MD, Hayes DN. ConsensusClusterPlus: a class discovery tool with confidence assessments and item tracking. Bioinformatics. 2010; 26:1572–3. https://doi.org/10.1093/bioinformatics/btq170 PMID:20427518

25. Hänzelmann S, Castelo R, Guinney J. GSVA: gene set variation analysis for microarray and RNA-seq data. BMC Bioinformatics. 2013; 14:7. https://doi.org/10.1186/1471-2105-14-7 PMID:23323831

26. Meng Z, Ren D, Zhang K, Zhao J, Jin X, Wu H. Using ESTIMATE algorithm to establish an 8-mRNA signature prognosis prediction system and identify immunocyte infiltration-related genes in Pancreatic adenocarcinoma. Aging (Albany NY). 2020; 12:5048–70. https://doi.org/10.18632/aging.102931 PMID:32181755

27. Yu G, Wang LG, Han Y, He QY. clusterProfiler: an R package for comparing biological themes among gene clusters. OMICS. 2012; 16:284–7. https://doi.org/10.1089/omi.2011.0118 PMID:22455463

28. Mayakonda A, Lin DC, Assenov Y, Plass C, Koeffler HP. Maftools: efficient and comprehensive analysis of somatic variants in cancer. Genome Res. 2018; 28:1747–56. https://doi.org/10.1101/gr.239244.118 PMID:30341162

29. Geeleher P, Cox N, Huang RS. pRRophetic: an R package for prediction of clinical chemotherapeutic response from tumor gene expression levels. PLoS One. 2014; 9:e107468. https://doi.org/10.1371/journal.pone.0107468 PMID:25229481

30. Petitprez F, Meylan M, de Reyniès A, Sautès-Fridman C, Fridman WH. The Tumor Microenvironment in the Response to Immune Checkpoint Blockade Therapies. Front Immunol. 2020; 11:784. https://doi.org/10.3389/fimmu.2020.00784 PMID:32457745

31. Cao R, Yuan L, Ma B, Wang G, Tian Y. Tumour microenvironment (TME) characterization identified prognosis and immunotherapy response in muscle-invasive bladder cancer (MIBC). Cancer Immunol Immunother. 2021; 70:1–18. https://doi.org/10.1007/s00262-020-02649-x PMID:32617668

32. Zeng D, Wu J, Luo H, Li Y, Xiao J, Peng J, Ye Z, Zhou R, Yu Y, Wang G, Huang N, Wu J, Rong X, et al. Tumor microenvironment evaluation promotes precise checkpoint immunotherapy of advanced gastric cancer. J Immunother Cancer. 2021; 9:e002467. https://doi.org/10.1136/jitc-2021-002467 PMID:34376552

33. Song P, Li W, Guo L, Ying J, Gao S, He J. Identification and Validation of a Novel Signature Based on NK Cell Marker Genes to Predict Prognosis and Immunotherapy Response in Lung Adenocarcinoma by Integrated Analysis of Single-Cell and Bulk RNA-Sequencing. Front Immunol. 2022; 13:850745. https://doi.org/10.3389/fimmu.2022.850745 PMID:35757748

34. Shi X, Dong A, Jia X, Zheng G, Wang N, Wang Y, Yang C, Lu J, Yang Y. Integrated analysis of single-cell and bulk

RNA-sequencing identifies a signature based on T-cell marker genes to predict prognosis and therapeutic response in lung squamous cell carcinoma. Front Immunol. 2022; 13:992990.
https://doi.org/10.3389/fimmu.2022.992990
PMID:36311764

35. Han L, Korangath P, Nguyen NK, Diehl A, Cho S, Teo WW, Cope L, Gessler M, Romer L, Sukumar S. HEYL Regulates Neoangiogenesis Through Overexpression in Both Breast Tumor Epithelium and Endothelium. Front Oncol. 2021; 10:581459.
https://doi.org/10.3389/fonc.2020.581459
PMID:33520697

36. Wang Z, Chen W, Zuo L, Xu M, Wu Y, Huang J, Zhang X, Li Y, Wang J, Chen J, Wang H, Sun H. The Fibrillin-1/VEGFR2/STAT2 signaling axis promotes chemoresistance via modulating glycolysis and angiogenesis in ovarian cancer organoids and cells. Cancer Commun (Lond). 2022; 42:245–65.
https://doi.org/10.1002/cac2.12274 PMID:35234370

37. Gao H, Liang J, Duan J, Chen L, Li H, Zhen T, Zhang F, Dong Y, Shi H, Han A. A Prognosis Marker SLC2A3 Correlates With EMT and Immune Signature in Colorectal Cancer. Front Oncol. 2021; 11:638099.
https://doi.org/10.3389/fonc.2021.638099
PMID:34211835

38. Zhang L, Wang Y, Song M, Chang A, Zhuo W, Zhu Y. Fibronectin 1 as a Key Gene in the Genesis and Progression of Cadmium-Related Bladder Cancer. Biol Trace Elem Res. 2023; 201:4349–59.
https://doi.org/10.1007/s12011-022-03510-1
PMID:36471209

39. Fu F, Yang X, Zheng M, Zhao Q, Zhang K, Li Z, Zhang H, Zhang S. Role of Transmembrane 4 L Six Family 1 in the Development and Progression of Cancer. Front Mol Biosci. 2020; 7:202.
https://doi.org/10.3389/fmolb.2020.00202
PMID:33015133

40. Lin B, Zhang T, Ye X, Yang H. High expression of EMP1 predicts a poor prognosis and correlates with immune infiltrates in bladder urothelial carcinoma. Oncol Lett. 2020; 20:2840–54.
https://doi.org/10.3892/ol.2020.11841
PMID:32782602

41. Zhang J, Zhou Q, Xie K, Cheng L, Peng S, Xie R, Liu L, Zhang Y, Dong W, Han J, Huang M, Chen Y, Lin T, et al. Targeting WD repeat domain 5 enhances chemosensitivity and inhibits proliferation and programmed death-ligand 1 expression in bladder cancer. J Exp Clin Cancer Res. 2021; 40:203.
https://doi.org/10.1186/s13046-021-01989-5
PMID:34154613

42. Xie R, Cheng L, Huang M, Huang L, Chen Z, Zhang Q, Li H, Lu J, Wang H, Zhou Q, Huang J, Chen X, Lin T. NAT10 Drives Cisplatin Chemoresistance by Enhancing ac4C-Associated DNA Repair in Bladder Cancer. Cancer Res. 2023; 83:1666–83.
https://doi.org/10.1158/0008-5472.CAN-22-2233
PMID:36939377

43. Oh DY, Fong L. Cytotoxic CD4+ T cells in cancer: Expanding the immune effector toolbox. Immunity. 2021; 54:2701–11.
https://doi.org/10.1016/j.immuni.2021.11.015
PMID:34910940

44. Farhood B, Najafi M, Mortezaee K. CD8+ cytotoxic T lymphocytes in cancer immunotherapy: A review. J Cell Physiol. 2019; 234:8509–21.
https://doi.org/10.1002/jcp.27782
PMID:30520029

45. Ozga AJ, Chow MT, Luster AD. Chemokines and the immune response to cancer. Immunity. 2021; 54:859–74.
https://doi.org/10.1016/j.immuni.2021.01.012
PMID:33838745

46. Li Y, Yang X, Su LJ, Flaig TW. VEGFR and EGFR inhibition increases epithelial cellular characteristics and chemotherapy sensitivity in mesenchymal bladder cancer cells. Oncol Rep. 2010; 24:1019–28.
https://doi.org/10.3892/or.2010.1019 PMID:20811684

47. Zhou X, Chen Y, Wang F, Wu H, Zhang Y, Liu J, Cai Y, Huang S, He N, Hu Z, Jin X. Artesunate induces autophagy dependent apoptosis through upregulating ROS and activating AMPK-mTOR-ULK1 axis in human bladder cancer cells. Chem Biol Interact. 2020; 331:109273.
https://doi.org/10.1016/j.cbi.2020.109273
PMID:33002460

48. Bhattacharjee S, Sullivan MJ, Wynn RR, Demagall A, Hendrix AS, Sindhwani P, Petros FG, Nadiminty N. PARP inhibitors chemopotentiate and synergize with cisplatin to inhibit bladder cancer cell survival and tumor growth. BMC Cancer. 2022; 22:312.
https://doi.org/10.1186/s12885-022-09376-9
PMID:35321693

Supplementary Figures
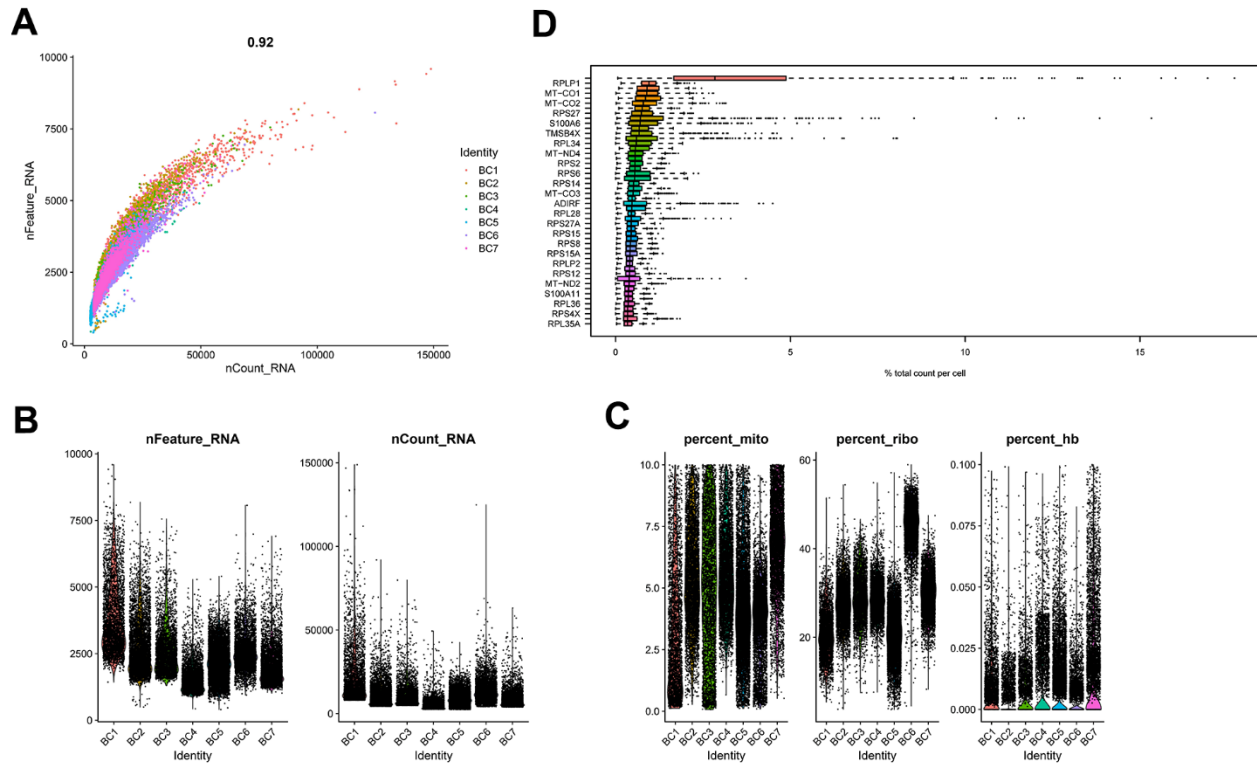
Supplementary Figure 1. Quality control of scRNA-seq data. (**A**) Correlation between nFeature_RNA and nCount_RNA. (**B**, **C**) Information of filtered scRNA-seq data from 7 BLCA samples. (**D**) The top 25 genes with the highest percentage of cellular expression.
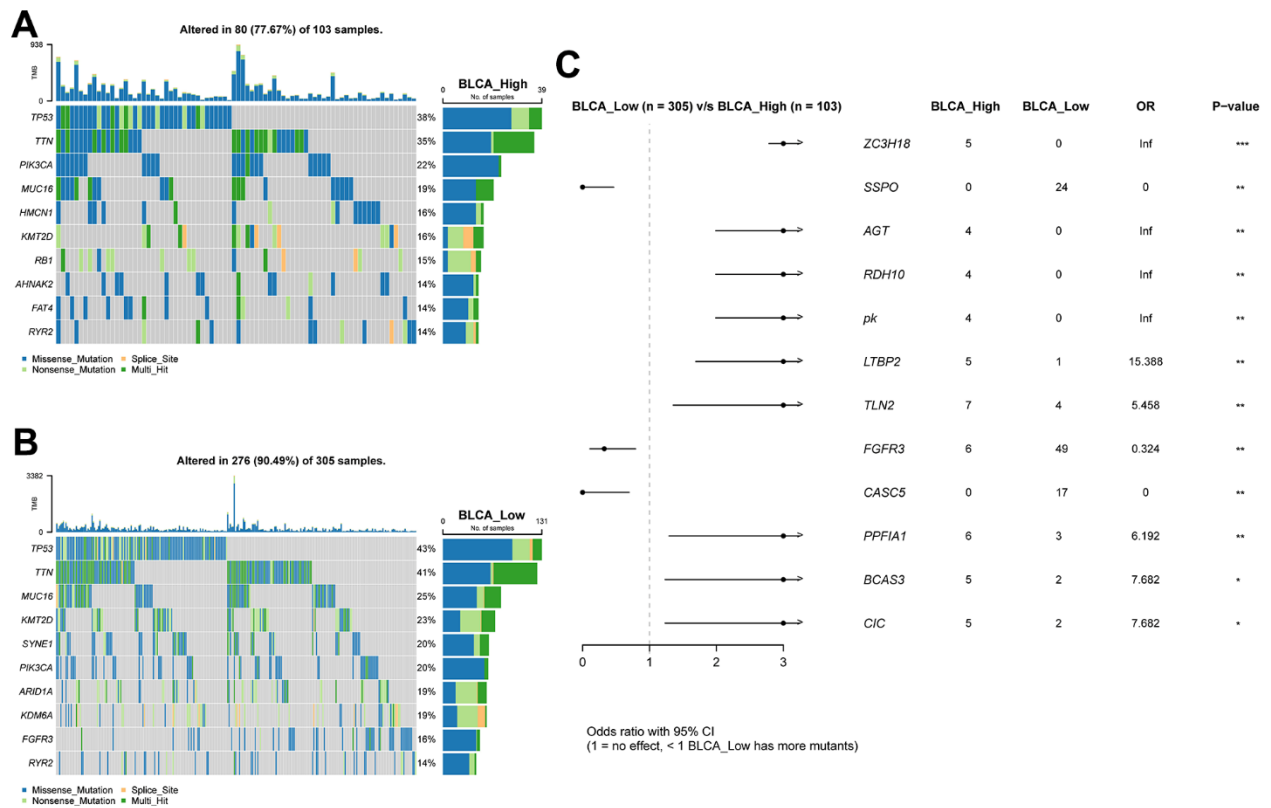
Supplementary Figure 2. Gene mutations in the high- and low-score groups. (**A**, **B**) Distribution of gene mutations in the high- and low-score groups. (**C**) Comparison of the gene mutations in the high- and low-score groups.
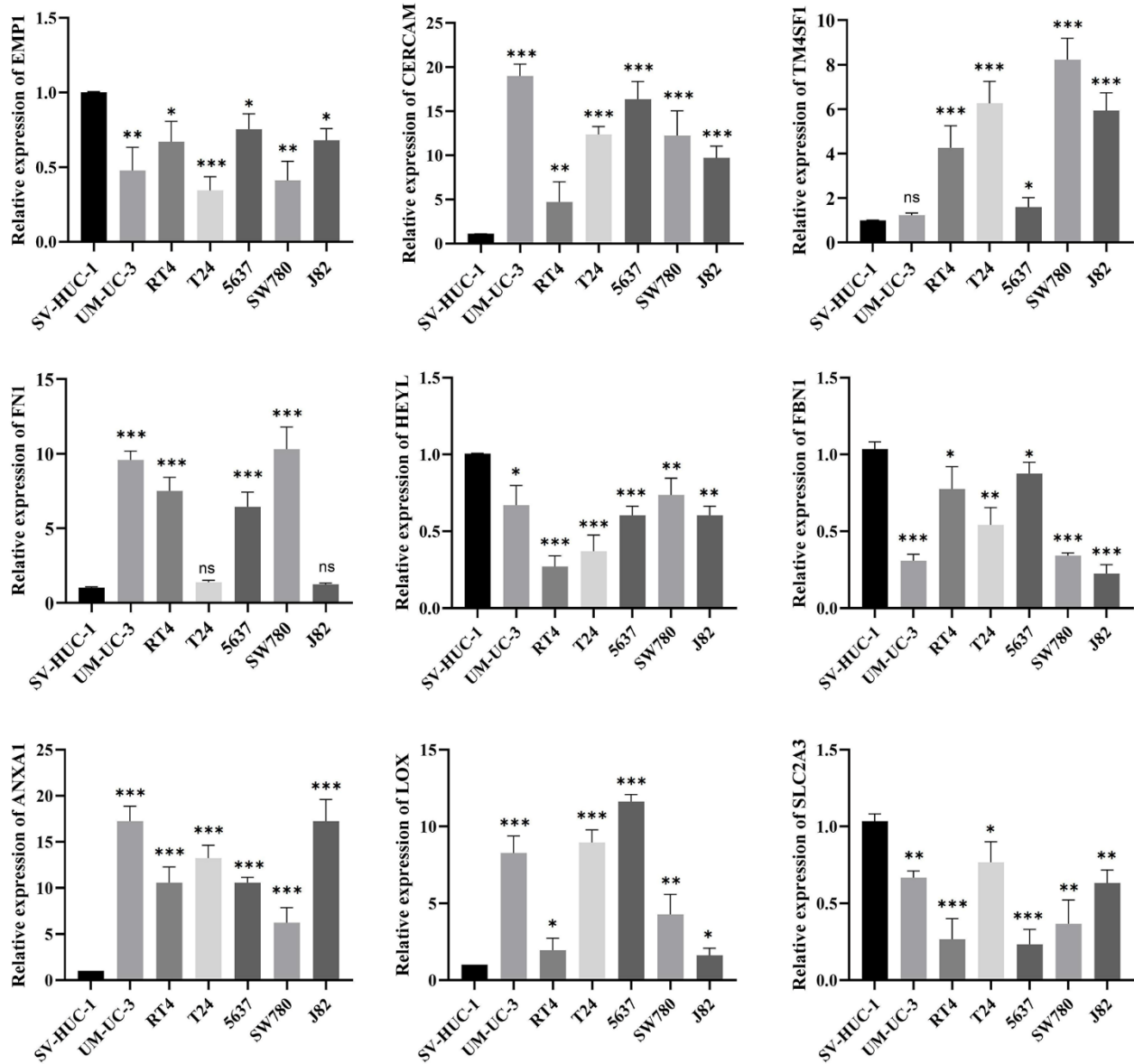
Supplementary Figure 3. mRNA expression levels of model genes in bladder uroepithelial cell line (SV-HUC-1) and BLCA cells (UM-UC-3, RT4, T24, 5627, SW780, and J82).
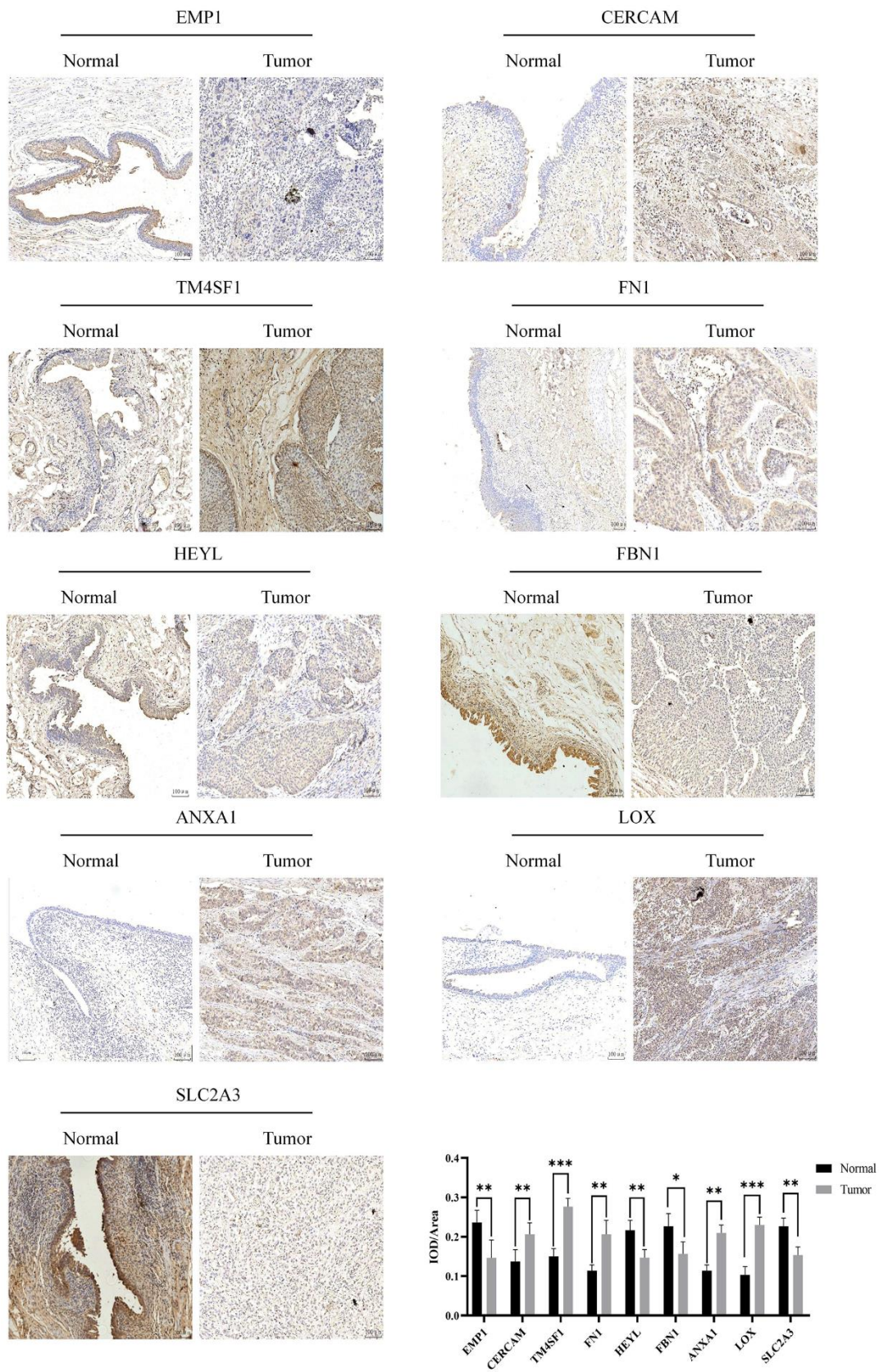
Supplementary Figure 4. Reprehensive image of the expression of model genes in tumor and paired normal samples revealed by IHC.

Supplementary Tables

Please browse Full Text version to see the data of Supplementary Table 2.

Supplementary Table 1. Primer sequences in RT-qPCR.

	Forward primer	Reverse primer
EMP1	GTGCTGGCTGTGCATTCTTG	CCGTGGTGATACTGCGTTCC
CERCAM	GAGCCCAGGTTCTACCCAGAT	GCAGAGTCTGATTGTTGGTCA
TM4SF1	TGCATCGGACATTCTCTGGTG	GTTCCAGCCCAATGAAGACAA
FN1	CGGTGGCTGTCAGTCAAAG	AAACCTCGGCTTCCTCCATAA
HEYL	GGAAGAAACGCAGAGGGATCA	CAAGCGTCGCAATTCAGAAAG
FBN1	TTTAGCGTCCTACACGAGCC	CCATCCAGGGCAACAGTAAGC
ANXA1	GCGGTGAGCCCCTATCCTA	TGATGGTTGCTTCATCCACAC
LOX	CGGCGGAGGAAAACTGTCT	TCGGCTGGGTAAGAAATCTGA
SLC2A3	GCTGGGCATCGTTGTTGGA	GCACTTTGTAGGATAGCAGGAAG
GAPDH	CCCACTCCTCCACCTTTGAC	CCACCACCCTGTTGCTGTAG

Supplementary Table 2. A detailed list of differential genes.